

Microporous annealable particles as embedding baths for multiscale vascular 3D bioprinting

Lucy Y. Tao

MSc thesis in Biomedical Engineering

Microporous annealable particles as embedding baths for multiscale vascular 3D bioprinting

by

Lucy Y. Tao

to obtain the degree of

Master of Science

at the Delft University of Technology,

to be defended publicly on Friday 28 April 2023 at 9:00 AM.



Student: Lucy Yiming Tao, 4550684
Project duration: March 28, 2022 – March 28, 2023

Thesis committee:	Prof. dr. A. A. Zadpoor	TU Delft	Chair
	Dr. ir. E. L. Fratila-Apachitei	TU Delft	Supervisor
	Dr. J. C. H. Leijten	UTwente	Supervisor
	Ir. M. R. Schot	UTwente	Daily supervisor
	Ir. M. L. Becker	UTwente	Daily supervisor
	Dr. J. Zhou	TU Delft	Committee member

An electronic version of this thesis is available at <http://repository.tudelft.nl/>.

Lucy Y. Tao was born in Nijmegen, the Netherlands in 1997. She earned her Dutch VWO gymnasium high school degree at Dominicus College Nijmegen in 2016. There, she participated in various extracurricular masterclasses including a two-year excellence program at Radboud University. In 2019, she received her BSc degree from Amsterdam University College (joint program with UvA and VU). She also completed additional courses from Fudan University Shanghai and the University of Sydney. Her BSc thesis in oral cell biology was conducted at the Academic Centre for Dentistry in Amsterdam and published in *Frontiers in cell developmental biology*.



She completed the courses for her bridging program and MSc degree in biomedical engineering at Technical University Delft, specialising in neuromusculoskeletal biomechanics. Her MSc thesis on tissue engineering was conducted at the University of Twente. Lucy will become the third member of her family to receive a MSc degree from TU Delft, following her father Dr.ir. Guoqiao Tao, 陶国桥 and sister Ir. Yida Tao, 陶一达 .

**UNIVERSITY
OF TWENTE.**

The work in this thesis was carried out at the department of Developmental Bioengineering (DBE) in the faculty of Science and Technology (TNW) at the University of Twente in Enschede, the Netherlands.

Preface

Before you lies the master thesis "Microporous annealable particles as embedding baths for multiscale vascular 3D bioprinting". This thesis is submitted in fulfillment of the graduation requirements of the Biomedical Engineering program at the Technical University of Delft, the Netherlands. The research was conducted in the Leijten Lab at the Developmental BioEngineering (DBE) group of the University of Twente, the Netherlands.

From my BSc internship in cell biology, I discovered my passion for conducting research, and over time, I developed an ambitious dream of developing human organs from stem cells in the lab for transplantation. To achieve my goal, I searched for research groups in tissue engineering and found the DBE group in Enschede, where I was fortunate enough to be accepted for an on-site internship position by Dr. Jeroen Leijten, for which I am very grateful. I was thrilled to have the opportunity to learn from two experienced PhD candidates, Maik Schot and Malin Becker, who generously shared their expertise with me.

While in Enschede, some unexpected events occurred in my personal life. Living far away from my fiancé was challenging, especially when I developed severe COVID symptoms. However, I was grateful to have made many great friends at the ballroom dancing association *4 happy feet*, which I did not expect. They provided me with much joy during dance classes, dinners, and movienights, and they even brainstormed on some of the technical future aspects of my thesis with me, particularly on the microvascular techniques for attaching my structure *in vivo*. I am especially grateful to Fiona, who not only taught me how to become a better dancer, but also how to make graphs in SPSS and improve images in PowerPoint for this thesis. Furthermore, I would like to acknowledge the efforts of Dennis along with the help of amongst others Harriet, Jimmy, and Thomas for "sabotaging" my work, because the more time I need to graduate, the longer I would stay with them in Enschede.

I sincerely hope you will enjoy reading the thesis report. It is my hope that the work presented in this thesis will contribute to future developments in tissue engineering and ultimately lead to the fully biofabricated kidneys for transplantation that I dream of.

Lucy Y. Tao

陶一明

Enschede, March 2023

Contents

Abstract	1
Keywords	1
1 Introduction	3
2 Materials and methods	7
2.1 List of materials	8
2.2 Microgel production with In-Air Microfluidics (IAMF)	8
2.3 Fluorescent alginate (Alg-F) synthesis and analysis	9
2.4 ATA synthesis.	9
2.5 UV-VIS spectrometry	11
2.6 MAP formation through photocrosslinking of microgels.	11
2.7 Developing print bath moulds	11
2.8 Fabricating print baths	11
2.9 Bulk ATA fabrication through photocrosslinking	12
2.10 Emb3D printing of perfusable channels in ATA	12
2.11 Swelling of ATA channels.	13
2.12 Interface trials between fluid Alg and microgels	14
2.13 Stability of Alg in an APTS	14
2.14 Degree of pre-saturation for a connected structure	14
2.15 Effect of needle movement on the self-healing properties of the microgel bath	15
2.16 Effect of microgel packing on the self-healing properties of the microgel bath	16
2.17 Printing and perfusion of final construct.	16
3 Results	19
3.1 Fabrication of a microporous structure with a high density capillary-like network	19
3.2 Fabrication of stable and perfusable channels in bulk hydrogel	20
3.3 Separating the MAP and liquid hydrogel through APTS	22
3.4 Printing through the interface and perfusing the structure	25
4 Discussion	29
5 Conclusion	37
Acknowledgements	38
Disclosure statement	38
References	49
A Schematic overview of experiments needed to build the final construct	51

B	Manual print trials in DexTA	53
C	Additional data from perfusion studies	55

Abstract

Vascularisation is a critical factor in large-scale tissue engineering, as it supports the survival of cells in large tissue constructs. In native tissue, a hierarchical vascular network is present where larger vessels transport nutrients and oxygen throughout the body, and smaller capillaries facilitate blood-tissue exchange. In large-scale engineered tissue, such a functional hierarchical vascular network is necessary for cell survival. In this study, we aimed to create a high-density capillary network using biocompatible hydrogels for tissue engineering purposes.

To achieve this, we first synthesised alginate-tyramine (ATA) by modifying the alginate backbone to contain tyramine groups. Then, we created monodisperse ATA microgels through in-air microfluidics (IAMF). These microgels were in turn used to form a microporous annealed particle (MAP) structure through photocrosslinking, which resulted in a structure containing the desired high-density microporous network.

Next, we showed that we could use embedded 3D (emb3D) printing techniques to fabricate channels in the ATA hydrogel, which we stabilised through photocrosslinking. These macroscale channels proved to be open and perfusable.

To create a stable interface between the microgels and hydrogel, we pre-saturated the microgels with a polymeric solution that forms an aqueous two-phase system (ATPS) with the ATA hydrogel. The ATPS and pre-saturation successfully counteracted capillary forces, keeping the hydrogel outside the microgel compartment. At the same time, the ATPS allowed the hydrogel and microgels to be in contact with each other, at which interface photocrosslinking was allowed to establish a connected structure.

By combining these approaches, we were able to successfully assemble a perfusable hierarchical porous network with micro- and macroscale vasculature. Specifically, we fabricated a macroscale channel using emb3D printing methods in a bath with both hydrogel and microgel components, which we then solidified through photocrosslinking. The resulting MAP was perfused through the macroscale inlet with fluorescent particles, demonstrating successful perfusion through the printed channel.

To date, the fabrication and perfusion of a multiscale vascular tree has not been demonstrated in this manner. Our study demonstrates the possibility for multiscale vascular emb3D printing through a microporous bath and highlights the potential of this innovative approach to overcome current limitations in tissue engineering.

Keywords

Tissue engineering, perfusable multiscale vasculature, high-density interconnected microporous network, embedded 3D printing.

1

Introduction

Organ shortage is a significant global healthcare problem worldwide. It is estimated that the number of organ transplantations performed represents less than 10% of the global need [1]. Furthermore, the gap between the number of patients in need of organs and the number of available organs for transplantation is increasing every year [2], [3]. Tissue engineering offers a potential solution to this problem by providing an alternative means to create replacement organs or tissues [4]–[8]. Apart from posing a solution to the problem of organ shortage for transplantation, engineered tissue can have various applications. For example, engineered tissue could reduce the number of animal tests in the drug development process [9], [10], help develop personalised medicine [11], [12], be used in disease modelling [4], [13], and be cultured for consumption [14]–[17].

Current research has shown the possibility of fabricating small 3D organoids that mimic the structure and function of an organ [18]. While organoids have shown great potential in disease modelling and drug testing [19], the production of larger anatomically relevant sized organs for transplantation remains a major challenge.

Vasculature plays a crucial role in the success of large-scale tissue engineering, as it enables the survival of cells in large tissue constructs. The human body's tissues receive nutrients and oxygen via a hierarchical vascular tree, where large vessels are responsible for transport through the body and capillaries facilitate blood-tissue exchange. In the human body, these large vessels consist of arteries with a diameter from 400 μm to 8 mm [20]. Intermediate vessels such as arteries and venules typically have a diameter of 40-300 μm [20]. The small capillaries typically have an inner diameter of 5 μm , although capillaries with a diameter of up to 40 μm can be found in the liver [20], [21]. To engineer large tissues, a comparable and functional vascular network is crucial [7]. The goal of this study is to create such a functional vascular network from biocompatible materials.

The creation of hollow structures resembling macroscale vessels in engineered tissues can be achieved through the use of 3D printing techniques [22]–[24]. However, it is important to note that the absence of a microscale capillary-like network in large engineered tissues results in a necrotic core and tissue death [25], [26], as cells require adequate oxygen and nutrient supply as well as metabolic waste removal for survival. The diffusion limit for these essential substances is limited to 100-200 μm in tissues [20]. The fabrication of such high-density and high-resolution open channels cannot be feasibly achieved using 3D bio-printing techniques and has thus not been reported. This highlights the need for further

advancements in the field to replicate the high-density capillary networks present in the human body. We propose to address this challenge by exploiting the dense and interconnected microporous network that is inherently present in microporous annealed particles (MAPs) [27]–[33]. In particular, we propose to use microgels in which cells can be encapsulated with sizes within the diffusion limit. Previous studies have demonstrated the successful encapsulation of cells within such microgels, which maintained cell viability [34]–[37].

To fabricate such a perfusable microporous structure connected to macroscale channels, we propose a four-step plan. The first step is to manufacture a MAP with a high-density capillary-like network from microgels. The second step is to fabricate perfusable arteriole-like channels using 3D printing techniques. The third step is to create a stable interface between the microgels from the first step and the hydrogel from the second step, so that it is possible to fabricate a channel that was connected to the MAP. In the fourth step, the approaches from the previous three steps are to be combined to assemble a perfusable hierarchical porous network (Fig. 1.1; Appendix A; Fig. A.1).

For the first step (Fig. 1.1), we chose to use a hydrogel that is biocompatible and double-crosslinkable for making such a MAP, where the first crosslinking mechanism is used to fabricate microgels from liquid hydrogel and the second crosslinking mechanism is used to fabricate MAPs from microgels. More specifically, we propose to make microgels from alginate (Alg) through in-air ionic crosslinking, which is faster and cleaner than conventional emulsion microfluidics [34]. The properties of Alg can be modified by functionalising the Alg-backbone [38]–[46]. When the Alg-backbone is functionalised with tyramine (TA), it gains dual crosslinking properties as the TA groups from the alginate-tyramine (ATA) can form covalent bonds between the microgels [47]–[50]. This second photocrosslinking step is used to form the MAP.

To achieve perfusion in the MAP, the presence of perfusable macroscale in- and outlets are necessary. This allows for the perfusion of the interstitial spaces between the microgels, ensuring that all cells have access to a sufficient blood supply within the diffusion limit. Furthermore, keeping transplantation in mind as a future application, these in- and outlets must be connected to the host's native vasculature through microvascular surgical methods to achieve perfusion. Therefore, it is necessary to connect the MAP to a macroscale perfusable channel.

To create perfusable arteriole-like channels (step 2, Fig. 1.1), we propose to fabricate channels by liquid-in-liquid embedded 3D printing (emb3D printing) based on an aqueous two-phase system (ATPS), where a sacrificial ink is printed in a supporting and curable hydrogel bath [51]. It has been reported that channels ranging from 18 μm to 600 μm in diameter can be fabricated using the emb3D printing method [22], [52], [53]. Keeping in mind that these channels must be connected to the MAP and the MAP is formed by crosslinking TA groups, a biocompatible crosslinkable material was needed that could be collected in liquid form in contact with ATA microgels. Preferably, the channels would be fabricated in a TA-crosslinkable material, so that channel fabrication and MAP formation could be completed simultaneously. For this purpose, we chose to fabricate the channels in ATA with the same visible light crosslinker as for the MAP fabrication.

To fabricate a structure in which the MAP and channel are connected and perfusable, first the microgels and liquid hydrogel are collected, then the open perfusable channel is fabricated through emb3D printing, and finally, the entire structure is solidified through

photocrosslinking in a one-step procedure. In this design, we exploit the self-healing properties of the microgel bath during channel fabrication [54]–[58], as emb3D printing will take place both through the ATA hydrogel and the microgels. From the moment the materials are collected to the materials are solidified through photocrosslinking, it is necessary to have a stable the interface between the microgels and liquid hydrogel.

We propose to stabilise the interface between the MAP and hydrogel with an ATPS (step 3, Fig. 1.1). The basic principle behind ATPS is the creation of two immiscible aqueous phases by mixing two polymers with different molecular weights and chemical properties in water, without diluting either of the polymeric solutions [59]–[61]. When the two solutions are brought together, phase separation will occur with a well-defined interface between them. This liquid-liquid interface can be visualised, as these solutions will each have their own characteristic refractive indexes [62]–[65]. By pre-saturating the microgels with such a polymeric solution, it could form an ATPS with the liquid ATA, effectively keeping the ATA out of the MAP.

In this study, we intend to combine the key ideas as mentioned above by fabricating the MAP and emb3D printed perfusable channel together in an ATPS (step 4, Fig. 1.1). With this approach, we aim to fabricate a perfusable and hierarchical vascular architecture using biocompatible materials.

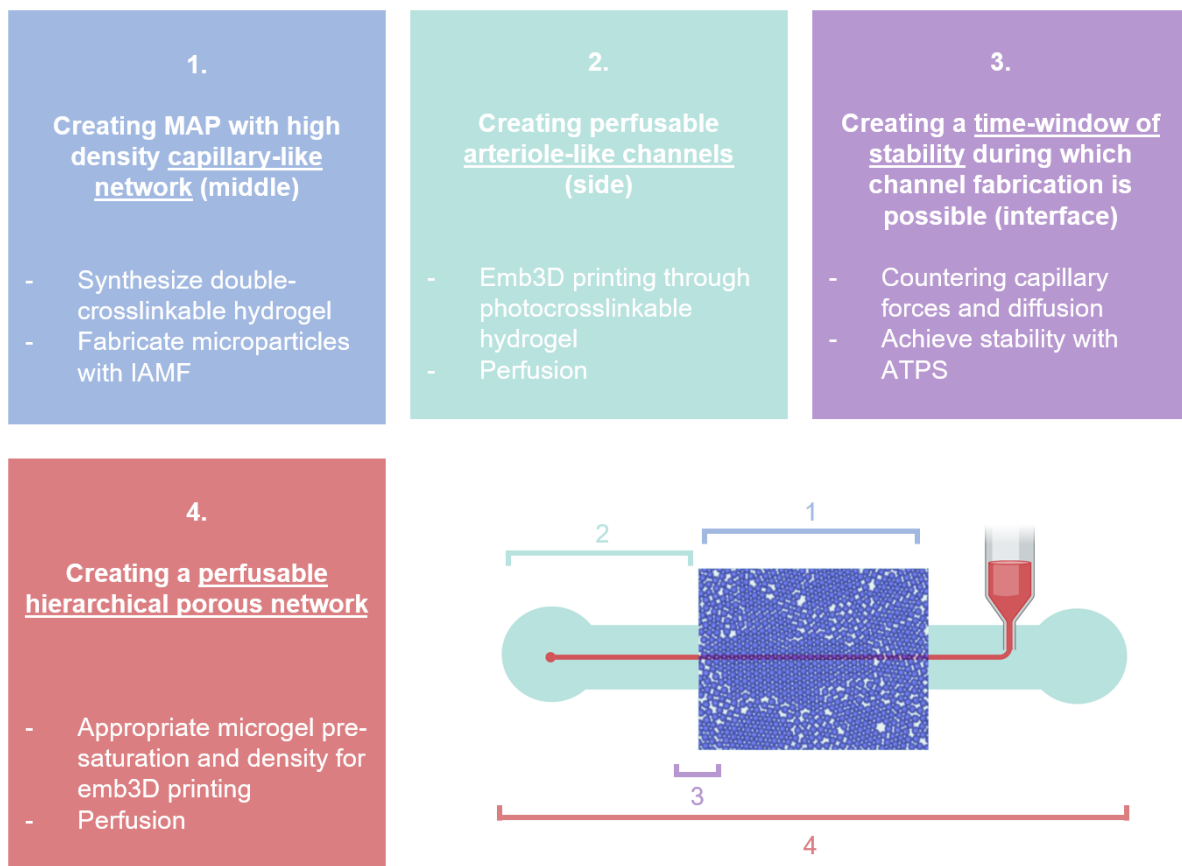


Figure 1.1: The fabrication of a perfusable hierarchically vascular network in four steps: (1) creating a microporous network from microgels; (2) creating macroscale channels in hydrogel; (3) creating stability between the microgels and hydrogel when they are brought together together; (4) fabricating a perfusable macroscale channel connected to a high density microporous capillary-like network.

2

Materials and methods

This chapter provides a detailed description of the experimental design and methods used to carry out the research. This chapter will start by listing the materials used in this study (section 2.1). Then, the methods related to step 1, creating a MAP with a high density capillary-like network, will be described (sections 2.2 - 2.6). This will be followed by the methods used in step 2, creating perfusable arteriole-like channels (sections 2.7 - 2.11) and step 3, creating a time-window of stability during which channel fabrication is possible (sections 2.12 - 2.14). Finally, the experiments for creating a perfusable hierarchical porous network will be described (sections 2.15 - 2.17).

2.1. List of materials

Material	Full name	Manufacturer
6-aminofluorescein	6-aminofluorescein	Sigma-Aldrich (USA)
Alg	Sodium Alginate (80 to 120 cP)	Wako Chemicals (USA)
CaCl ₂	Calcium chloride dihydrate	Sigma-Aldrich (USA)
Clear Resin	Clear Resin V4 (liquid photopolymer)	Formlabs Inc. (USA)
DexTA	Dextran-tyramine	Synthesized by MB
DMEM	Dulbecco's Modified Eagle Medium	Gibco (USA)
DMTMM	4-(4,6-Dimethoxy-1,3,5-triazin-2-yl)-4-methylmorpholinium chloride	Fluorochem (UK)
EDC	N-(3-Dimethylaminopropyl)-N'-ethylcarbodiimide hydrochloride	Sigma-Aldrich (USA)
EtOH	Ethanol	
FBS	Fetal Bovine Serum	Sigma-Aldrich (USA)
Fitc-dex 2000kDa	Fluorescein isothiocyanate-dextran average mol wt 2,000,000 Da	Sigma-Aldrich (USA)
Fluorescent particles	Fluorescent Airbrush Colors	Createx Colors (USA)
Food dye	Sodium chloride, E124, E102	TRS Food Colour (India)
Gelatin	Gelatin, tested according to Ph. Eur.	Sigma-Aldrich (USA)
H ₂ O ₂	Hydrogen peroxide 30 (w/w)	Sigma-Aldrich (USA)
HRP	Peroxidase from horseradish	Sigma-Aldrich (USA)
IPOH	Isopropanol	
MES	2-(N-morpholino)ethanesulfonic acid	Sigma-Aldrich (USA)
MetOH	Methanol	
NaCl	Sodium chloride	
NHS	N-Hydroxysuccinimide	Sigma-Aldrich (USA)
PBS	Phosphate buffered saline	Lonza (Switzerland)
PDMS elastomer base	Dowsil 184 Silicone Elastomer Base	Sylgard 184, Dow Corning (USA)
PDMS curing agent	Dowsil 184 Silicone Elastomer Curing	Sylgard 184, Dow Corning (USA)
PEG-35K	Polyethylene glycol 35000	Sigma-Aldrich (USA)
Pen/Strep	Penicillin Streptomycin	Gibco (USA)
RhodB	Rhodamine B	Sigma-Aldrich (USA)
RU	Ruthenium	Advanced BioMatrix (USA)
SPS	Sodium Persulfate	Advanced BioMatrix (USA)
TA	Tyramine hydrochloride, 99%	Acros Organics (China)

2.2. Microgel production with In-Air Microfluidics (IAMF)

The IAMF device, as developed by Visser *et al.* [34], generates monodisperse droplets by breaking up a liquid jet using the eigenfrequency of the fluid with a vibrating piezoelectric element. The liquid jet is formed by pushing liquid through a nozzle using a syringe pump (Fig. 2.1). The flow speed of the fluid is controlled with a syringe pump and compatible software (QMix, Cetoni GmbH, Germany). The position of the nozzles is monitored using an iDS camera (iDS Imaging Development Systems GmbH, Germany) compatible software (uEYE, iDS Imaging Development Systems GmbH, Germany).

The technique and settings for microgel production using 100 μm -diameter nozzles were optimised using a 0.5% w/v Alg in MilliQ water (MQ) solution and a 0.1 M CaCl₂ in MQ crosslinking solution with 10% EtOH to reduce the surface tension of the fluid. The Alg-solution was filtered using a 0.2 μm filter before microgel fabrication to prevent clogging of the nozzle. The flow speeds of both the Alg- and CaCl₂ jets were set to be 2000 $\mu\text{L}/\text{min}$. The offset was set to be 4 VdC and the amplitude was 4 Vpp. The frequency of

the vibrating piezo was found to be around 4.57 kHz, although this frequency was adjusted on the fly until a stable droplet train could be observed. The microgels were collected and kept in a 0.03 M CaCl₂ in MQ solution and stored at 4 °C. Microgel production with IAMF was also performed with (mixtures of) 0.5% w/v Alg derivatives, such as photocrosslinkable alginate-tyramine (ATA) or fluorescent alginate (Alg-F). Images of microgels were taken with an EVOS microscope and analysed using ImageJ software (NIH). Graphs were created using SPSS (IBM) and schematics were made with BioRender.

2.3. Fluorescent alginate (Alg-F) synthesis and analysis

Two protocols for the synthesis of Alg-F using 6-aminofluorescein were adjusted from literature [44], [45], resulting in the synthesis of Alg-F-MES and Alg-F-PBS (Fig. 3.1H).

Alg-F-MES was synthesized according to the protocol from *Balaj et al.* [44]. In short, 2.1 mL of 100 mM MES buffer (pH 4.98), 560 µL of 6-aminofluorescein in MetOH (30 mg/mL), 280 µL of EDC in 25 mM MES buffer (50 mg/mL, pH 4.98), and 280 µL of NHS in MQ (30 mg/mL) were added to 7 mL of 3% w/v Alg in MQ and stirred for 15 min at room temperature in the dark. The solution was then dialysed (Pre-wetted RC Tubing MWCO: 3.5kD, Spectra/Por 6 Dialysis Membrane, Repligen, USA) in the dark against MQ at 4 °C for 3 days with 4 changes of the dialysis bath, after which the product was freeze-dried and stored in the dark at room temperature.

Alg-F-PBS was synthesized according to the protocol from *Hori et al.* [45]. In short, 1 mL of 90 mM EDC in PBS and 1 mL of 90 mM NHS in PBS were added to 8 mL of 2.5% w/v Alg in PBS, achieving a 10 mL solution of 2% w/v Alg + 9 mM EDC + 9 mM NHS in PBS. This solution was stirred for 2 h at room temperature, after which 10 mL of 4.5 mM 6-aminofluorescein in 70% EtOH was added and stirred for 18 h at room temperature in the dark. The solution was then dialysed (Pre-wetted RC Tubing MWCO: 3.5kD, Spectra/Por 6 Dialysis Membrane, Repligen, USA) in the dark against MQ at 4 °C for 2.5 days with 5 changes of the dialysis bath, after which the product was freeze-dried and stored in the dark at room temperature. The yield of the synthesis was determined by weighing the Alg-F.

Microgels were made using IAMF from a solution consisting of 0.4% w/v Alg and 0.1% w/v Alg-F-PBS or Alg-F-MES in MQ, following the protocol described in section 2.2. The fluorescence of the microgels was attempted to visualise using an EVOS FL microscope and Zeiss LSM 880 confocal microscope.

2.4. ATA synthesis

Alg was modified to contain TA functional groups for photocrosslinkable properties (Fig. 3.2A). To do this, 2.2 g of TA was added to 500 mL of a 1% w/v solution of Alg in MQ for substitution catalysed by 3.5 g of DMTMM for 24 h under continuous stirring. After that, 40 mL of saturated NaCl in MQ was added to the solution for 30 min to help the precipitation. The precipitation took place in a fivefold volume of EtOH on ice under continuous stirring, after which it was stored overnight at 4 °C. To remove the EtOH, the samples were centrifuged for 5 min at 5000 rpm at 15 °C after which the samples were dried on a petridish in a desiccator at room temperature. Unreacted TA and other small molecules were then removed through dialysis (Pre-wetted RC Tubing MWCO: 3.5kD, Spectra/Por 6 Dialysis Membrane, Repligen, USA) against MQ for 4 d. Water was refreshed twice a day for the first two days (demi water)

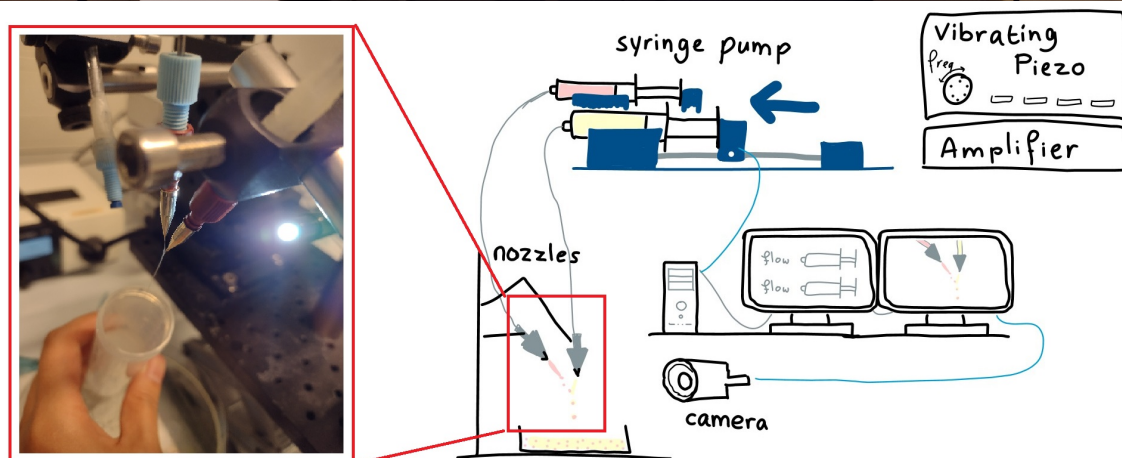


Figure 2.1: Top: overview photo of IAMF setup. Bottom left: photo of droplet train (left nozzle) and crosslinker (right nozzle) coming out of 100 μm IAMF nozzles for in-air crosslinking. Bottom right: Schematic of IAMF setup with labeled components of the setup.

and once a day for the last two days (MQ). The concentration of the solution was increased by evaporating the solvent using a vacuum rotary evaporator at 40 °C. Finally, the solution was freeze-dried and stored at room temperature for future use. The yield of the synthesis was determined by weighing the ATA. This protocol was carried out twice in parallel, hence resulting in two batches: ATA_A and ATA_B.

A smaller bath of ATA_S with the aim of a higher degree of TA substitution was made.

For this, 0.88 g of TA was added to 100 mL of 1% w/v solution of Alg in MQ for substitution catalysed by 1.4 g of DMTMM (double concentration as compared to the previous protocol) for 48 h under continuous stirring. After that, the solution was precipitated, centrifuged, desiccated, dialysed, freeze-dried, and stored according to the protocol described above.

2.5. UV-VIS spectrometry

The substitution percentage of TA on the synthesized ATA was determined using a Nanodrop spectrophotometer (ND-1000 spectrophotometer). The measurements were taken on wavelength $\lambda = 274$ nm, of which it is known that it is absorbed by TA. The degree of TA substitution was then calculated using a calibration curve.

2.6. MAP formation through photocrosslinking of microgels

Microgels produced with IAMF from 0.5% w/v ATA in MQ and 0.1% w/v Fitc-dex 2000kDa were annealed as reported in previous work [35]. In short, a mould was fabricated by drilling a hole of approximately 3 mm in diameter in a 1 mm thick plate. The microgels were collected in this hole on top of a glass plate. Excess fluid was taken up from the bottom of the mould with lint-free tissues. Solutions of 2 mM RU and 2 mM SPS were added on top of the microgels in succession, after which the structure was exposed to visible light (E27 807 lumen white LED lamp) for 15 min for photocrosslinking. To evaluate the photocrosslinking quality, the structure was taken up in MQ and exposed to mechanical turbulence to see whether the MAP would stay intact. The MAP was imaged with a Nikon A1 confocal microscope. The images were analysed with ImageJ (NIH) and Matlab (MathWorks). Graphs were created using Prism 5 (GraphPad).

2.7. Developing print bath moulds

3D CAD designs of the negative replica casting moulds for the print bath and compatible lid were designed in TinkerCAD (Autodesk). The designs were then loaded into PreForm software and printed with a Form3B+ freeform resin printer (Formlabs, USA) using Clear Resin at a layer thickness of 0.100 mm. The moulds were then soaked in IPOH for 15 minutes in the dark. After blow-drying the moulds with air, the moulds were again washed with IPOH using Form Wash (Formlabs, USA). When the moulds were clean, they were cured at 60 °C for 60 min by Form Cure (Formlabs, USA). To avoid confusion, definitions are given for the terms used in this report regarding the print bath, its origin (print bath mould), and its contents (hydrogels and microgels or construct) (Tab. 2.1).

2.8. Fabricating print baths

Initially, baths were made from polydimethylsiloxane (PDMS). To prepare PDMS, the elastomer base and curing agent were mixed by fiercely stirring in a 10:1 weight ratio. After fierce stirring, the mixture was degassed at -0.08 MPa for 1 h. This uncured PDMS could then be used immediately or stored at -18 °C for future use. Uncured PDMS at room temperature was poured onto the negative replica casting mould of the print bath and compatible lid, after which it was degassed in the desiccator at -0.08 mPa for 30 min and cured at 60 °C for 22-24 h. The bath and lid were carefully removed from the moulds with a surgical 22-blade, tweezers, and gentle pulling. Images were taken with an iDS camera (iDS UI-

Table 2.1: Terminology and definitions used in this report regarding the print bath, its origin (print bath mould), and its contents (hydrogels and microgels or construct).

Print bath mould	Mould for negative replica casting. Designed in TinkerCAD and fabricated with the freeform resin printer.
Print bath	PDMS or gelatin bath, result of negative replica casting. Holder for ATA hydrogel and microgels.
Hydrogels and microgels	Materials to fill the print bath. Materials through which emb3D printing is performed.
Construct	Solidified hydrogels and microgels after photocrosslinking, either with or without emb3D printed channel.

3140CP Rev 2, IDS Imaging Development Systems GmbH, Germany) and compatible uEYE software (IDS Imaging Development Systems GmbH, Germany). Schematics were created with BioRender.

Gelatin baths were also fabricated in the negative replica casting moulds from 10% w/v gelatin in PBS. Freshly dissolved gelatin at 37 °C was poured into the mould of the print bath and solidified for at least 30 min at 4 °C, after which the baths could be removed from the moulds using a wet spatula. During experiments, the gelatin baths were kept on ice. No gelatin lids were fabricated, as it was sufficient to directly pipet liquid gelatin on top of the gelatin bath to seal the structure.

2.9. Bulk ATA fabrication through photocrosslinking

To determine the photocrosslinking variables of the various ATA batches, 1% w/v ATA in MQ solutions were made and mixed with various photocrosslinker concentrations in the dark (1 mM RU and 5 mM SPS; 0.5 mM RU and 5 mM SPS; 0.5 mM RU and 2 mM SPS; 1 mM RU and 2 mM SPS). For every sample, 200 μ L was transferred to an Eppendorf cap (height: 2-3 mm) and exposed to visible light (Philips lamp, 4.3 W, 4000 K, 470 lm, 40 mA, 200-240 Vac, 50/60 Hz) from approximately 0.5-1 cm distance from the light source. The liquidity of the sample was evaluated every 30 sec by poking it with a pipette tip to determine the time needed for the ATA to solidify and to acquire sufficient stiffness to lift the sample from the bath.

2.10. Emb3D printing of perfusable channels in ATA

Emb3D printed channels were fabricated in the dark with a 25G nozzle to print through 1% w/v ATA_S with 0.5 mM RU and 5 mM SPS in MQ. The ink consists of 5% w/v PEG-35K and food dye in MQ to identify the channel during printing. Channels were made with various print speeds (100 mm/min, 200 mm/min, 300 mm/min, 400 mm/min, and 500 mm/min) and infusion rates (50 μ L/min, 100 μ L/min, and 200 μ L/min) after which they were fixed in the hydrogel through photocrosslinking (4000 K, 470 lm, 30 sec). The printing variables were controlled using an Inkredible+ 3D bioprinter (Cellink, Sweden) through a

G-code (Tab. 2.2). The infuse rate was controlled by a syringe pump (Harvard Apparatus, PHD Ultra, USA).

Table 2.2: G-Code used to fabricate 2 mm long channels. Post processed by INKREDIBLE post processor. External perimeters extrusion width = 0.28mm ($0.06\text{mm}^3/\text{s}$); perimeters extrusion width = 0.26mm ($0.05\text{mm}^3/\text{s}$); infill extrusion width = 0.26mm ($0.05\text{mm}^3/\text{s}$); solid infill extrusion width = 0.26mm ($1.04\text{mm}^3/\text{s}$); top infill extrusion width = 0.26mm ($1.04\text{mm}^3/\text{s}$).

G21		; set units to millimeters
G90		; use absolute coordinates
M83		; use relative distances for extrusion
G1	X-10 Y0 Z20	
G1	X-10 Z0.00 F1200.000	
G4	P6000	; pause needle movement to turn on extrusion
G1	X10 F100	; change F for different print speeds
G4	P3000	; pause needle movement to turn off extrusion
G1	X10 Z30 F1200.000	
G1	Y50 F1200.000	
M761		
G1	E-2.00000 F2400.00000	; retract extruder 0
M760		
G1	E2.00000 F2400.00000	; unretract extruder 0
M761		
G1	E-2.00000 F2400.00000	; retract extruder 0
G1	Z30	; move needle out of the way for photocrosslinking
M84		; disable motors

Before perfusion, an open outlet was created by cutting into the bulk hydrogel. Perfusion of the emb3D printed channel in ATA was completed by inserting a 32G needle into the closed inlet of the printed channel from the top and manually pushing fluorescent particles suspended in 5% w/v PEG-35K in MQ through it. The flow of the fluorescent particles was filmed using an Andonstar microscope (Shenzhen Andonstar tech Co., China) and the side view of the perfused channel was imaged using an EVOS FL microscope.

To analyse the channel sizes, the solidified structures were removed from the PDMS baths with a wet spatula, after which cross-sectional slices of the bulk hydrogel holding the channels were made using a surgical 22-blade. The slices were then taken up in MQ and immediately imaged using an Andonstar microscope (Shenzhen Andonstar Tech Co., China). Further analysis of the channel sizes was completed with ImageJ (NIH) and OriginPro (OriginLab Co.).

2.11. Swelling of ATA channels

Solutions of 1% w/v ATA_S, 0.5 mM RU, and 5 mM SPS were made in various solvents: MQ, PBS, or culture medium (89% DMEM, 10% FBS, and 1% Pen/Strep). The solutions were poured into a 1.2 mL mould (height: approximately 1 cm) with a needle (20G x 1" (0.9 x 25 mm), BD Microlance TM3, Switzerland) through the middle, after which it was exposed to visible light (4000 K, 470 lm) for 1 min 30 sec. Cross-sectional slices of the hydrogel were made using a surgical 22-blade. The slices were kept in various storage solutions (MQ,

PBS, or culture medium) at 37 °C. The size of the channel was evaluated at time points 0 min, 30 min, 1 h, 4 h, 6 h, 24 h, and 7 d using an EVOS microscope. Further analysis was completed with ImageJ (NIH) and OriginPro (OriginLab Co.). Schematics were created with BioRender.

2.12. Interface trials between fluid Alg and microgels

To observe the effect of capillary forces of the microgels on the liquid Alg, Alg microgels were strained and collected in the middle component of the PDMS bath. Some granules of RhodB were taken up in 1% w/v Alg in MQ, after which 60 μL of the Alg-solution was added in each side-compartments. Finally, the microgels were wetted with 80 μL MQ. The stability of the structure was monitored with an iDS camera (iDS UI-3140CP Rev 2, IDS Imaging Development Systems GmbH, Germany) and compatible uEYE software (IDS Imaging Development Systems GmbH, Germany) and analysed using ImageJ (NIH).

To observe the effect of diffusion, Alg microgels were strained and collected in the middle component of the PDMS bath after which 80 μL MQ was added on top. Then, some granules of RhodB were taken up in 1% w/v Alg in MQ and 60 μL of this Alg-solution was added in each side-compartments. The stability of the structure was monitored with an iDS camera (iDS UI-3140CP Rev 2, IDS Imaging Development Systems GmbH, Germany) and compatible uEYE software (IDS Imaging Development Systems GmbH, Germany) and analysed using ImageJ (NIH).

To observe the behaviour of liquid Alg and microgels in an ATPS system, Alg microgels were strained and taken up in 80 μL 5% w/v PEG-35K in MQ. After rigorous mixing, the pre-wetted microgels and storage fluid were collected in the middle compartment of the PDMS bath. Then, a spatula of dried green food dye was taken up in 1% w/v Alg in MQ, after which 60 μL of this solution was added in each side-compartments. The stability of the structure was monitored with an iDS camera (iDS UI-3140CP Rev 2, IDS Imaging Development Systems GmbH, Germany) and compatible uEYE software (IDS Imaging Development Systems GmbH, Germany) and analysed using ImageJ (NIH). Schematics were created with BioRender.

2.13. Stability of Alg in an ATPS

To study the interface stability of 1% w/v Alg and 5% w/v PEG-35K, Alg solutions in MQ or PBS were stacked in a cuvette on top of various PEG-35K solutions in MQ or PBS. The shadows of the polymer solutions and their interface based on refractive indexes were continuously monitored for the first 30 min. After the initial 30 min, the shadows were monitored in intervals. For this, an iDS camera (iDS UI-3140CP Rev 2, IDS Imaging Development Systems GmbH, Germany) and compatible uEYE software (IDS Imaging Development Systems GmbH, Germany) were used. The shadow was cast using a light source near the camera (Fig. 2.2). The images were analysed using ImageJ (NIH). Schematics were created with BioRender.

2.14. Degree of pre-saturation for a connected structure

ATA microgels were washed, strained, and taken up in 20 μL 5 mM RU, 50 mM SPS, and 5% w/v PEG-35K in PBS while being kept in the dark. After rigorous mixing, the pre-

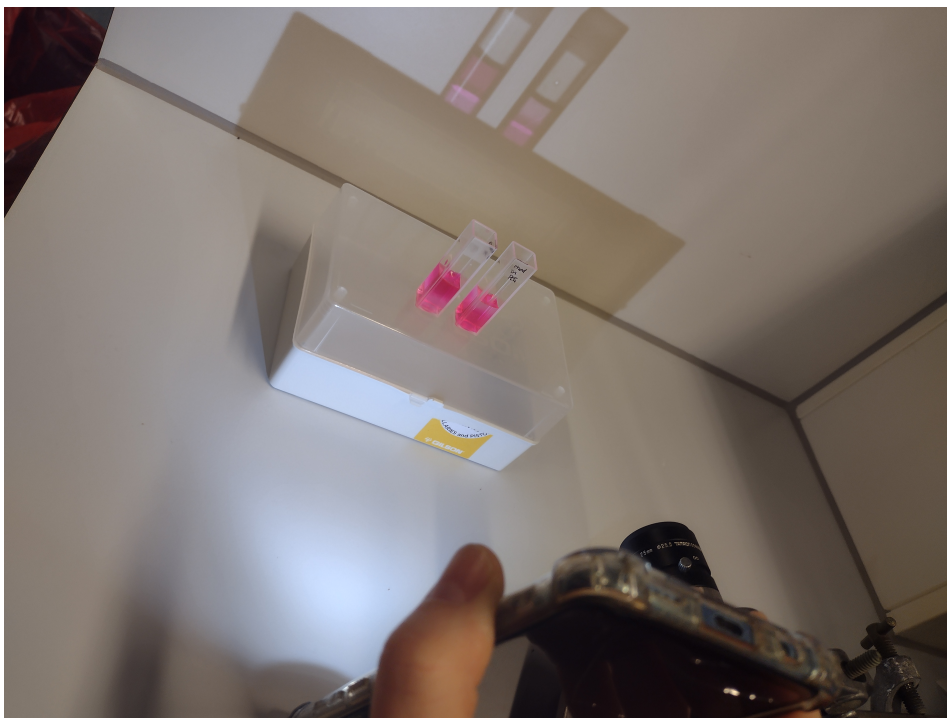


Figure 2.2: Photo of the ATPS interface test setup. In this image, the Alg solutions are coloured and the PEG solutions were initially clear, although diffusion of the RhodB colouring is observed. A shadow of the cuvettes was cast where the ATPS interface was clearly visualised despite the diffusion of the colouring agent. The photo is taken with the camera of a mobile phone.

wetted microgels were collected in the middle compartment of the PDMS bath. Then, 60 μL of 0.5 mM RU, 5 mM SPS, and 1% w/v ATA_S in PBS was added in each of the side-compartments. The structure was exposed to visible light (4000 K, 470 nm) for 1 min 30 sec for photocrosslinking. The connection between the MAP and bulk ATA was tested using gravitational and hydrodynamic forces. Imaging was completed with an iDS camera (iDS UI-3140CP Rev 2, IDS Imaging Development Systems GmbH, Germany) and compatible uEYE software (IDS Imaging Development Systems GmbH, Germany) as well as an EVOS microscope.

2.15. Effect of needle movement on the self-healing properties of the microgel bath

To evaluate the effect of needle movement on the self-healing properties of the microgel bath, Alg microgels were washed, strained, and taken up in 20 μL 5% w/v PEG-35K. After rigorous mixing, the pre-wetted microgels were collected in the middle compartment of the PDMS bath with a spatula. Then, 60 μL of RhodB-stained 1% w/v Alg in PBS was added in each of the side-compartments. A needle (25G needle, BD Microlance TM3, Switzerland) was dragged through the structure at various movement speeds (50 mm/min, 100 mm/min, 200 mm/min, 400 mm/min, 600 mm/min, 800 mm/min, and 1000 mm/min) using an Inkredible+ 3D bioprinter (Cellink, Sweden) (Fig. 2.3), during which the self-healing capacities of the microgel-bath were observed by eye.

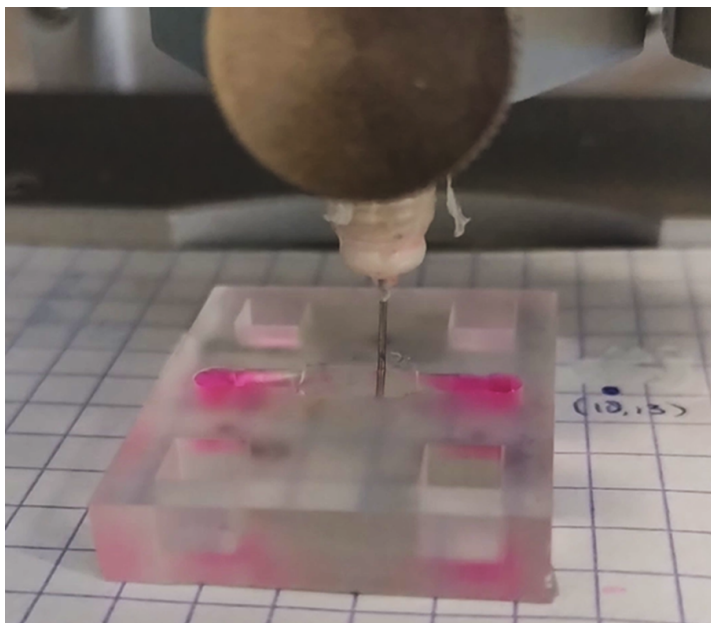


Figure 2.3: Image from a video where the 25G needle from the Inkredible+ printer is moving through the bath filled with RhodB-stained Alg and microgels from left to right. The video was made with the camera of a mobile phone.

2.16. Effect of microgel packing on the self-healing properties of the microgel bath

To show the effect of microgel packing on the self-healing properties of the microgel bath, ATA microgels were washed, strained, and taken up in 5 mM RU, 50 mM SPS, and 2, 20, or 200 μL 5% w/v PEG-35K in PBS while being kept in the dark. After rigorous mixing, the pre-wetted microgels and suspension fluids were collected in the middle compartment of the PDMS bath. Then, 60 μL of 0.5 mM RU, 5 mM SPS, and 1% w/v ATA_S in PBS was added in each of the side-compartments. A needle (25G needle, BD Microlance TM3, Switzerland) was dragged through the structure at $f = 100$ mm/min using an Inkredible+ 3D bioprinter (Cellink, Sweden). The structure was exposed to visible light (4000 K, 470 lm, 30 sec) for photocrosslinking. The crosslinked structure was transferred on top of a spatula and images were taken using an iDS camera (iDS UI-3140CP Rev 2, IDS Imaging Development Systems GmbH, Germany) and compatible uEYE software (IDS Imaging Development Systems GmbH, Germany).

2.17. Printing and perfusion of final construct

ATA microgels were washed, strained, and taken up in 20 μL 5 mM RU, 50 mM SPS, and 5% w/v PEG-35K in PBS while being kept in the dark. After rigorous mixing, the pre-wetted microgels were collected in the middle compartment of a gelatin bath. Then, 60 μL of 0.5 mM RU, 5 mM SPS, and 1% w/v ATA_S in PBS was added in each of the side-compartments.

Channels were emb3D printed through a 25G needle with fluorescent particles and food dye suspended in 5% w/v PEG-35K in PBS at a print speed of 100 mm/min using an Inkredible+ 3D bioprinter (Cellink, Sweden) and an infuse rate of 50 $\mu\text{L}/\text{min}$ using a syringe pump (Harvard Apparatus, PHD Ultra, USA). The structure was then photocrosslinked with visi-

ble light (4000 K, 470 lm, 30 sec) and sealed with a liquid gelatin coating, which was solidified and kept on ice until perfusion and imaging.

Before perfusion, one end of the hydrogel was cut to create an open outlet. Perfusion fluid was prepared by straining (70 μm) fluorescent particles suspended in 5% w/v PEG-35K. Perfusion of the emb3D printed channel in ATA was completed manually using a 32G needle which entered the inlet of the channel from the side of the gelatin bath.

The perfused structures were macroscopically visualised using an iDS camera (iDS UI-3140CP Rev 2, IDS Imaging Development Systems GmbH, Germany) with compatible uEYE software (IDS Imaging Development Systems GmbH, Germany) while exposed to UV light (Hamamatsu LightningCure LC8) and microscopically analysed using a Nikon A1 confocal microscope and ImageJ software (NIH). Schematics were created with BioRender.

3

Results

3.1. Fabrication of a microporous structure with a high density capillary-like network

This study aimed to fabricate a biocompatible microgel-based structure with a high-density capillary-like network. To achieve this goal, biocompatible Alg-microgels were fabricated with IAMF (Fig. 3.1A) where a continuous Alg droplet train is ionically crosslinked (Fig. 3.1B) in the air (Fig. 3.1C). When comparing IAMF (flow rate: 2000 $\mu\text{L}/\text{min}$) to conventional emulsion microfluidics (flow rate: 8 $\mu\text{L}/\text{min}$), a 250-fold increase in the production speed of microgels is found in our lab in terms of volume (Fig. 3.1E). The IAMF-fabricated microgels were monodisperse with a diameter of 114 μm (SD 2.6) and roundness of 0.87 (SD 0.047, n=146) (Fig. 3.1D, F-G).

To make the microgels visible under a laser-scanning confocal microscope, the Alg backbone was functionalised with 6-aminofluorescein (Fig. 3.1H). Fluorescent alginate (Alg-F) was synthesized using two distinct protocols in literature, resulting in Alg-F-MES and Alg-F-PBS. No fluorescence for either the Alg-F-MES or Alg-F-PBS microgels was detected using EVOS microscopy. The results showed that the Alg-F synthesis in MES buffer resulted in 3x stronger fluorescence compared to synthesis in PBS buffer when visualised with the Zeiss confocal microscope using the same settings (Fig. 3.1I-K): their respective mean grey values are 11.660 for Alg-F-PBS and 37.323 for Alg-F-MES. The yield for Alg-F-MES was 71% and the yield for Alg-F-PBS was 78%.

To ensure that the MAP maintained its shape, the microgels were made photocrosslinkable by functionalizing the Alg backbone with TA (Fig. 3.2A-B). The synthesis yielded 56.0% ATA_A, 55.5% ATA_B, and 73.1% ATA_S. The results showed that the degree of TA synthesis was about 4.7 % for the 24-hour synthesis protocol and about 7.0 % for the 48-hour synthesis protocol (Fig. 3.2C-E). Photocrosslinking of ATA microgels was successful and resulted in a microporous structure (Fig. 3.2F). The average pore size was 64.17 μm and the median void space in the MAP structure was 12.48 %, which corresponds to a range of capillary- and arteriole-sized vessels in the human body (Fig. 3.2G-H). About 31% of these pores range from 5-40 μm in diameter and correspond to native human capillary-sized pores.

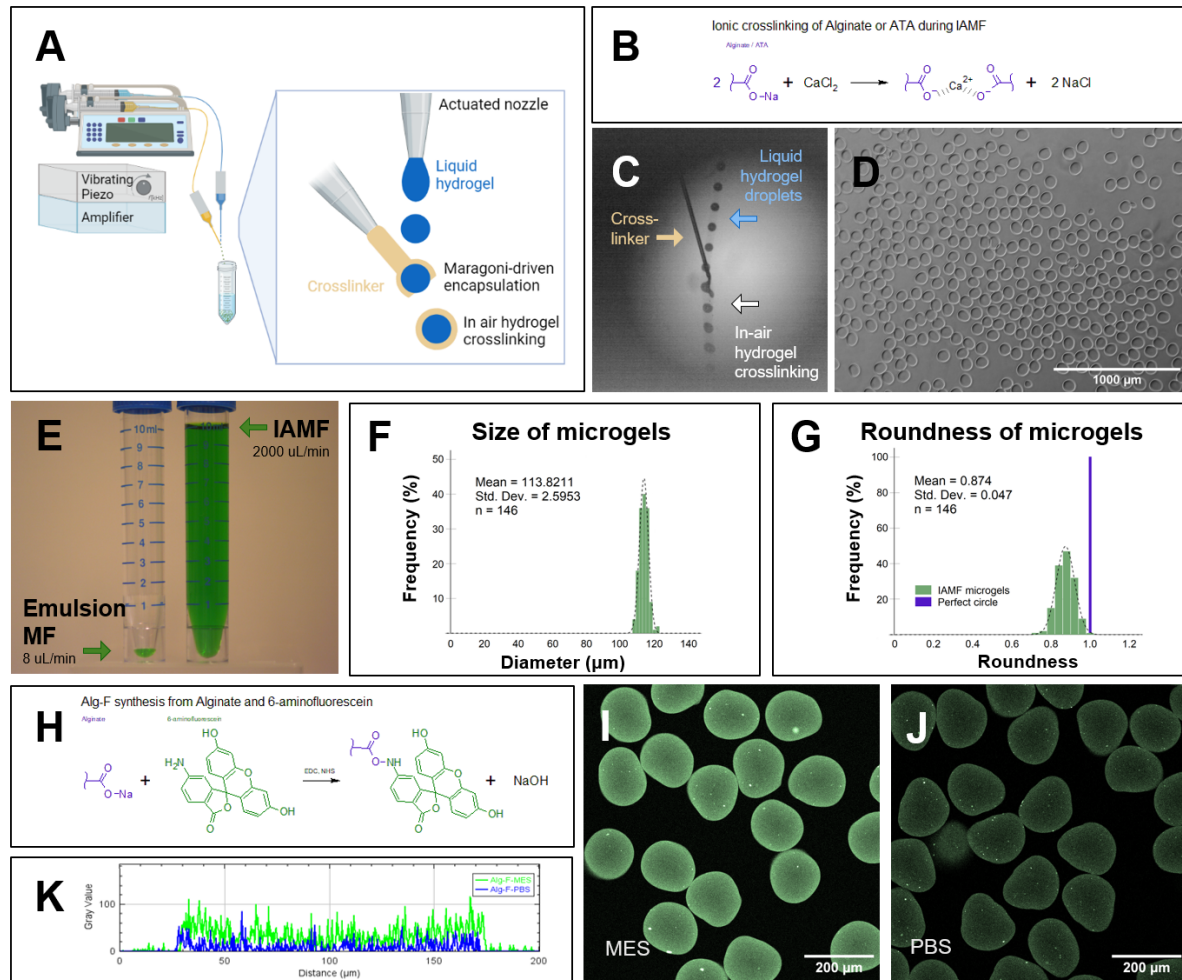


Figure 3.1: The fabrication of microgels. **(A)** Schematic illustration of the production of microgels with IAMF. **(B)** Chemical structures of Alg (or Alg derivative, purple) under influence of calcium-chloride during microgel fabrication using IAMF. **(C)** Microscopic image of liquid hydrogel droplets and crosslinker during IAMF. **(D)** Monodisperse microgels fabricated by IAMF with the 100 μm nozzle. **(E)** Quantification of the volume of microgels that can be produced in 5 minutes with conventional emulsion microfluidics at 8 $\mu\text{L}/\text{min}$ and IAMF at 2000 $\mu\text{L}/\text{min}$. **(F)** Size and **(G)** roundness distribution of microgels fabricated by IAMF with a 100 μm nozzle ($n = 146$) where a high average value of 87.4% (4.7 pp) for roundness combined with a low standard deviation of 2.6 μm for the average diameter indicates that the microgels are monodisperse. **(H)** Chemical structures of the synthesis of Alg-F from Alg (purple) and 6-aminofluorescein (green) under influence of EDC and NHS. Microgels made from Alg-F synthesized with the **(I)** MES and **(J)** PBS buffer as observed using a Zeiss LSM 880 microscope. **(K)** Grey value analysis of the fluorescent microgels quantifies a 3x stronger fluorescence in the Alg-F-MES microgels as compared to the Alg-F-PBS microgels.

3.2. Fabrication of stable and perfusable channels in bulk hydrogel

The purpose of the present study was to establish stable perfusable channels in ATA hydrogel. To achieve this goal, the photocrosslinking time was evaluated for various ATA batches. Also, the photocrosslinker concentrations required to solidify and gain sufficient stiffness were evaluated. It was known from preliminary studies that a concentration of 1 mM RU and 5 mM SPS is sufficient in similarly synthesized ATA batches. The aim of this study was to evaluate the performance of reduced photocrosslinker concentrations as high pho-

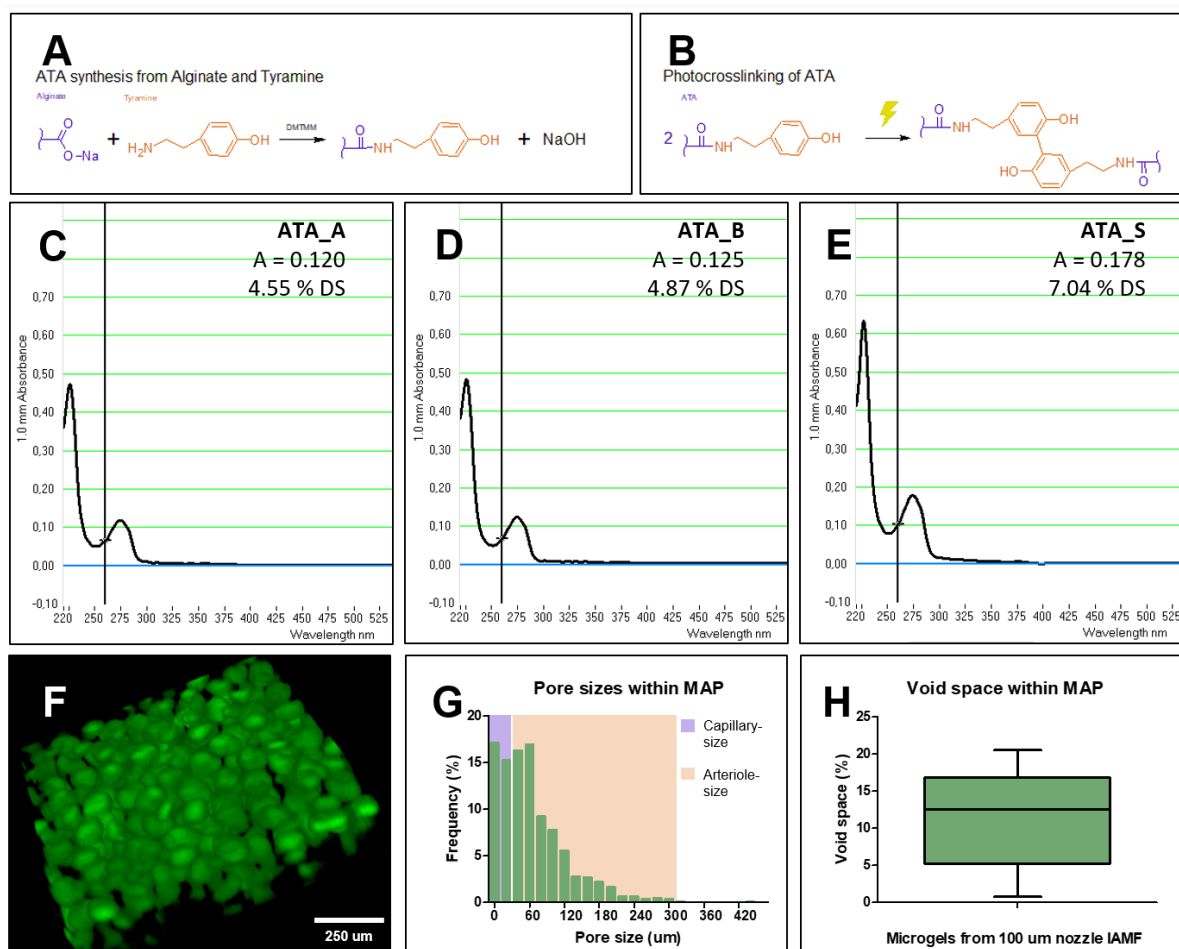


Figure 3.2: The creation of a MAP with a high-density capillary-like network. (A) Chemical structures of the synthesis of photocrosslinkable alginate from Alg (purple) and TA (orange) under the influence of DMTHM. (B) Chemical structures of the photocrosslinking process of ATA under influence of RU, SPS, and visible light. (C-E) Absorbance curves from UV-VIS spectrometry analysis for the various ATA batches. (F) MAP after photocrosslinking of ATA-microgels. (G) Pore size quantification within MAP, where the pore sizes are related to capillary- and arteriole-sizes in the human body. (H) Total void space quantification within the MAP, with a medium void space fraction of 12.48 %.

tocrosslinker concentrations are known to impact cell proliferation negatively. Also, it is essential to reach sufficient solidity and stiffness of the ATA within the time that the printed channel is stable. It was observed that with 0.5 mM RU and 5 mM SPS, the shortest time was required with the lowest amount of photocrosslinker concentrations (Tab. 3.1). Furthermore, it was indicated that the stiffness ATA_S was higher than that of ATA_A or ATA_B after 30 sec of exposure to light, however, measurements to confirm this observation are lacking. Nevertheless, it was decided to continue with ATA_S for channel fabrication.

Next, a swelling test with cross-sectional slices (Fig. 3.3A) was conducted to determine the most suitable hydrogel solvent and storage solution for long-term stability. The results showed that channels embedded in ATA_S dissolved in MQ displayed a higher degree of swelling over time (Fig. 3.3B-C) as compared to those embedded in ATA_S dissolved in PBS or culture medium (Fig. 3.3D-E). Further, the samples kept in MQ as a storage solution were observed to be less stable and more gel-like than those kept in PBS or culture medium (Fig. 3.3F). Based on these findings, it was concluded that both PBS and culture medium

Table 3.1: Time needed for various ATA batches with various photocrosslinker concentrations to solidify (first line) and gain sufficient stiffness to lift the sample from the mould (second line) through exposure to visible light (4000 K, 470 lm).

	0.5 mM RU 2 mM SPS	0.5 mM RU 5 mM SPS	1 mM RU 2 mM SPS	1 mM RU 5 mM SPS
ATA_A	2 min 30 sec 4 min	30 sec 30 sec	1 min 2 min	30 sec 30 sec
ATA_B	2 min 30 sec 3 min 30 sec	30 sec 30 sec	1 min 30 sec 2 min 30 sec	30 sec 30 sec
ATA_S	1 min 30 sec 1 min 30 sec	30 sec 30 sec	1 min 1 min 30 sec	30 sec 30 sec

would be excellent choices for dissolving the hydrogel and preserving the sample stability. Ultimately, for research purposes, PBS was selected as the solvent as well as the storage solution as it was both colourless and convenient.

Furthermore, the impact of various printing variables on the formation of open, thus perfusable channels was evaluated. The results indicated that the channel size increased with larger infuse rates ($i[\mu\text{L}/\text{min}]$) and/or lower print speeds ($f[\text{mm}/\text{min}]$). In particular, it was observed that the size of the open channel decreases when the print speed increases for both infuse rates $i = 50 \mu\text{L}/\text{min}$ (Fig. 3.3G-I) and $i = 100 \mu\text{L}/\text{min}$ (Fig. 3.3J-L). It must be noted that the channel stability was dependent on the printing parameters. Stable open channels were produced using the following parameters: (i) $i50f100-500$, (ii) $i100f400-500$, and (iii) $i200f400-500$ ($n = 3$), while channels produced in the 0.6 mm diameter range were perceived as less stable as one out of three samples broke during analysis for samples made with both $i50f50$ and $i200f300$ settings (Fig. 3.3M). Out of the stable open channels, it was found that the open channels produced at $i50f200-400$, $i100f300-500$, and $i200f500$ were arteriole-sized. Researchers observed better visualisation of perfusion in larger channels as opposed to smaller channels. Perfusion was observed macroscopically live from a top view (Fig. 3.3N) and microscopically in hindsight from a side view (Fig. 3.3O). Therefore, perfusion imaging of the channel (Fig. 3.3P-R) and further experiments were conducted using the $i50f100$ settings.

3.3. Separating the MAP and liquid hydrogel through ATPS

The objective of the present study was to investigate the stability and connection between the capillary-like structure and the liquid hydrogel. In the previous sections, the creation of a capillary-like structure and the establishment of perfusable channels in ATA was separately demonstrated. To perfuse the capillary-like structure, it is necessary to connect the perfusable channel to the capillary-like structure. To facilitate the collection of microgels and hydrogel, a bath was developed to collect the various materials, keeping the possibility of perfusion in mind. The bath was designed to consist of compartments for the MAP and the perfusable channels. For this bath, 3D CAD designs for the negative replica casting mould were created (Fig. 3.4A-B). From these negative moulds, PDMS baths and compatible lids (Fig. 3.4C-D) were fabricated with negative replica casting. The bath has showing a shallow rectangular compartment for the MAP with an inlet and outlet on opposite sides (Fig. 3.4E). The bath also featured a system to secure a compatible lid in place with a marked

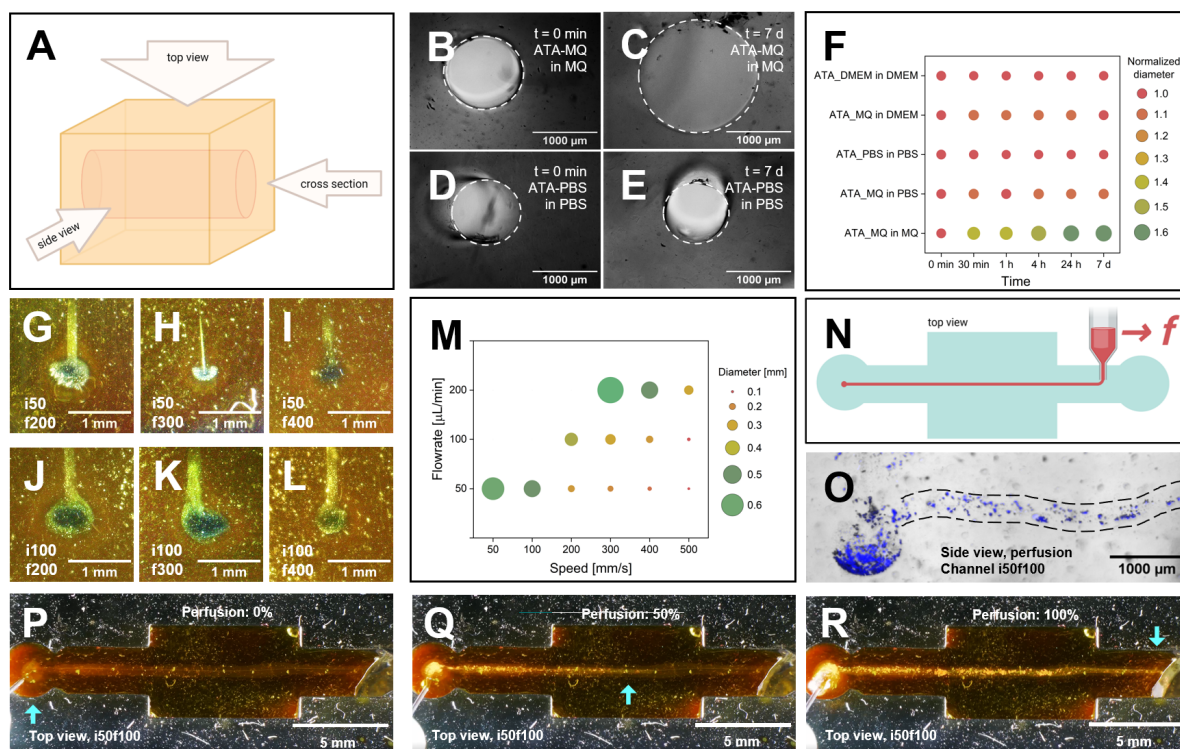


Figure 3.3: The creation of open perfusable channels in ATA hydrogel through emb3D printing and photocrosslinking. (A) Schematic relating the terminology *top view*, *side view*, and *cross section* to the orientation of the channel in the hydrogel. (B-E) Panel of cross-sectional images from the swelling study at various time points ($t = 0$ min and $t = 7$ d) and various hydrogel solvents and storage solutions (MQ and PBS). (F) Bubble graph with the results of the swelling test ($n = 3$). Swelling is observed over time when exposing the hydrogel to MQ. (G-L) Panel of cross-sectional images from the printed channel size study at various print speeds ($f = 200$ mm/min, $f = 300$ mm/min, $f = 400$ mm/min) and various infuse rates ($i = 50$ μ m/min and $i = 100$ μ m/min) ($n = 3$ for channels with a diameter of 0.5 mm or smaller, $n = 2$ for channels with a diameter of 0.6 mm or larger, $n = 0$ for empty spaces). (M) Bubble graph with the results of the printed channel size study ($n = 3$ for diameter < 0.6 mm, $n = 2$ or $n = 0$ for other). Larger channels are created with an increased infuse rate or decreased print speed. (N) Top-view schematic of the printing process through hydrogel in the mould. (O) Side-view fluorescent microscopic image of a printed and perfused inlet and channel. (P-R) Top-view images of the perfusion process through a printed channel from left to right, where the perfusion progress in each image is indicated with a blue arrow.

inlet and outlet for perfusion.

The initial observation when bringing together the microgels and liquid hydrogel was that the liquid hydrogel infiltrated the pores of the MAP due to capillary forces. Capillary forces are the attractive forces between a liquid and a solid surface that cause the liquid to rise or fall (Fig. 3.5A). In our case, the stacked microgels exert these capillary forces on the liquid hydrogel, rendering the capillary-like structure no longer microporous after photocrosslinking (Fig. 3.5J). To resolve this, infiltration was blocked by pre-saturating the MAP with MQ. However, it was observed that the MQ in the MAP diluted the liquid hydrogel on the interface due to diffusion (Fig. 3.5D, K; Appendix B).

Therefore, it was attempted to pre-saturate the MAP with a polymeric solution to prevent interaction between the liquid hydrogel and the MAP through achieving ATPS stability (Fig. 3.5B). The study focused on the stability of the ATPS interface between 1% w/v Alg and 5% w/v PEG-35K in MQ and PBS. In particular, the study aimed to create a window

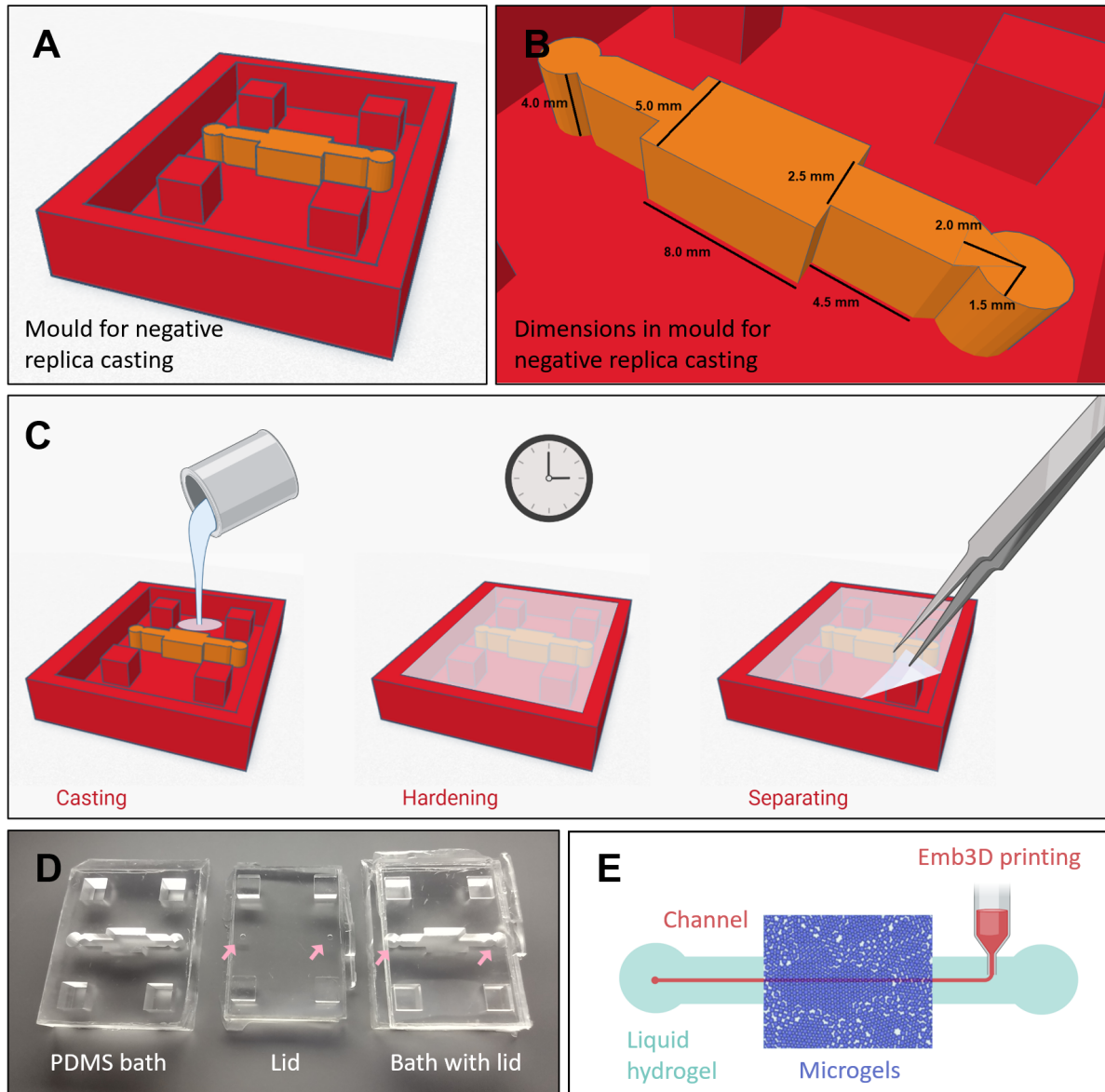


Figure 3.4: (A) 3D CAD design for 3D printing a mould for negative replica casting with a print-bath component (orange) and empty cubes to make it compatible to secure a lid (red cubes). (B) Dimensions of the print bath component in the negative 3D CAD design. (C) Three steps for negative replica casting: pouring the PDMS or gelatin (left), hardening the material by baking PDMS or cooling gelatin (middle), and gently separating the solidified bath from the mould (right). (D) PDMS products of the mould (left), compatible lid (middle) with marked positions for in- and outlets (pink arrows), and both the mould and lid put together (right). (E) The intended purposes of the bath components were the microgels are collected in the middle compartments and the liquid hydrogel is collected in the side compartments. For research purposes, emb3D printing can be completed in a straight line in this bath.

of ATPS stability that allows for emb3D printing of a channel through the combined structure. Visualisation of the ATPS interface was based on a difference in refractive indexes of the polymeric solutions (Fig. 3.5C).

The results showed that ATPS stability was observed when stacking Alg dissolved in MQ (Alg_MQ) on top of PEG-35K dissolved in MQ (PEG_MQ) solutions for over 2 hours but less than 24 hours (Fig. 3.5E). However, no ATPS stability was observed when stacking Alg_PBS

on top of PEG_MQ, as the interface between the two liquids immediately merged into each other (Fig. 3.5F-G). Limited ATPS stability was observed between Alg_PBS and PEG_PBS, as the PEG-35K solution penetrated the Alg solution in slow swirling movements (Fig. 3.5H-I).

The time window of ATPS stability necessary for embedded 3D printing through the construct in this study was found to be less than 5 minutes, for which both the purely MQ and PBS ATPS systems were suitable (Fig. 3.5E, H). The results also showed that when the MAP was pre-saturated with a 5% w/v PEG-35K solution, the liquid ATA formed a clear interface with the PEG-35K and stayed out of the MAP (Fig. 3.5L).

Finally, observations indicated that with the appropriate amount of pre-saturation, it was possible to establish a connection between the MAP and the liquid ATA with a clear interface between the two components, which remained connected even when balanced on a spatula in the air (Fig. 3.5M) or dropped in PBS (Fig. 3.5N).

3.4. Printing through the interface and perfusing the structure

This study aimed to create open perfusable channels using emb3D printing techniques through the liquid hydrogel, ATPS interface, and microgel bath (Fig. 3.6A). To achieve this goal, the response of the microgels to needle movement was evaluated first. The results showed that the packing of the microgels plays a crucial role in determining the outcome of the experiment (Fig. 3.6C). If the microgels were densely packed, the self-healing properties of the microgel bath were lost, leading to deformation of the structure upon needle movement. Conversely, if the microgels were suspended and not in contact with each other, photocrosslinking between the microgels was unsuccessful. It was found that the addition of $20\mu\text{L}$ fluid to $140\mu\text{L}$ freshly strained and therefore loose-packed microgels was sufficient to create a self-healing, photocrosslinkable bath. This corresponds to a total suspension volume of $160\mu\text{L}$ with roughly 110K $114\mu\text{m}$ diameter microgels and a packing density of approximately 60% [66]. After we found the appropriate amount of pre-saturation, studies were completed to find the appropriate print-speed range in which the microgel bath has self-healing properties. We found that needle movements between 50-800 mm/min were compatible for this purpose.

In the next experiment, researchers attempted to perfuse the MAP through a channel in a PDMS bath. The results indicated that the perfusion particles traversed the channel (Appendix C; Fig. C.1A), but instead of entering the MAP, they took the path of least resistance along the edges between the MAP and the bath (Appendix C; Fig. C.1B). In response to this observation, researchers restricted the void space near the edges of the construct and increased friction between the microgels and the bath by switching from PDMS to a gelatin bath and cover (Fig. 3.6B). The results showed that perfusion particles were able to successfully enter the MAP through the channel (Fig. 3.6D). The locations of the channel in the hydrogel and the interface between the hydrogel and MAP are both identifiable in a microscopic brightfield 3D reconstruction (Fig. 3.6E). It is observed that in the bulk-hydrogel compartment, the red particles used in perfusion are aligned in the channel, while in the MAP compartment, the red particles distribute throughout the structure (Fig. 3.6F). The 3D results showed perfusion particles in the channel (Fig. 3.6G) and in the MAP around the particles (Fig. 3.6H).

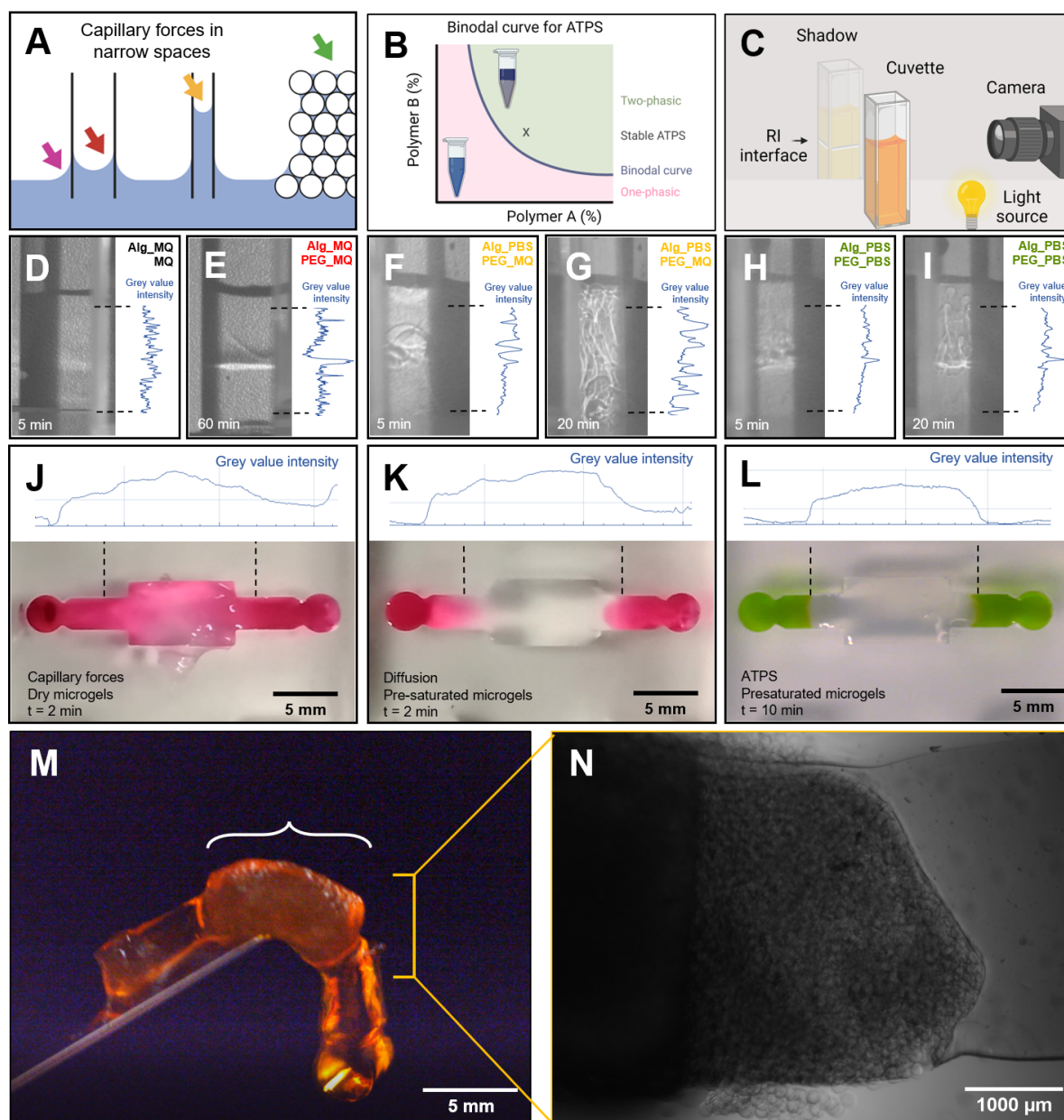


Figure 3.5: The creation of a stable interface between the liquid hydrogel and the microgels. **(A)** Schematic explanation of fluid movement through narrow spaces due to capillary forces based on cohesion, adhesion and surface tension at the coloured arrows. **(B)** Schematic of a binodal curve for achieving ATPS. **(C)** Schematic of the experimental setup for visualising and studying the ATPS interface. **(D)** Shadow of ATPS study at $t = 5$ min where 1% w/v Alg dissolved in MQ is stacked on top of MQ. No ATPS is observed. **(E)** Shadow of ATPS study at $t = 60$ min where 1% w/v Alg dissolved in MQ is stacked on top of 5% w/v PEG dissolved MQ. Stable ATPS is observed. **(F-G)** Shadow of ATPS study at **(F)** $t = 5$ min and **(G)** $t = 20$ min where 1% w/v Alg dissolved in PBS is stacked on top of 5% w/v PEG dissolved MQ. ATPS is observed with unstable interface between phases. **(H-I)** Shadow of ATPS study at **(H)** $t = 5$ min and **(I)** $t = 20$ min where 1% w/v Alg dissolved in PBS is stacked on top of 5% w/v PEG dissolved PBS. ATPS is observed with decreased stability of the interface over time. **(J-L)** Top: grey value analysis over the length of the bath. Bottom: various configurations with liquid Alg and microgels: Alg (pink) penetrating dry microgels (white) due to capillary forces at $t = 2$ min **(J)**; Dilution of Alg (pink) at the interface by MQ between the microgels (white) due to diffusion at $t = 2$ min **(K)**; 1% w/v Alg (green) and pre-saturated microgels with 5% w/v PEG-35K (white) stay separated due to ATPS at $t = 10$ min **(L)**. Dotted lines at the interfaces of the liquid hydrogel and microgels. **(M)** Side-view macroscopic image of a solidified connected structure due to ATPS and photocrosslinking balanced on a spatula to show the connectivity. **(N)** Side-view microscopic image of a solidified connected structure stored in PBS. The connection is created by ATPS and photocrosslinking where a clear interface is visible between the capillary-like structure (left) and the bulk hydrogel (right).

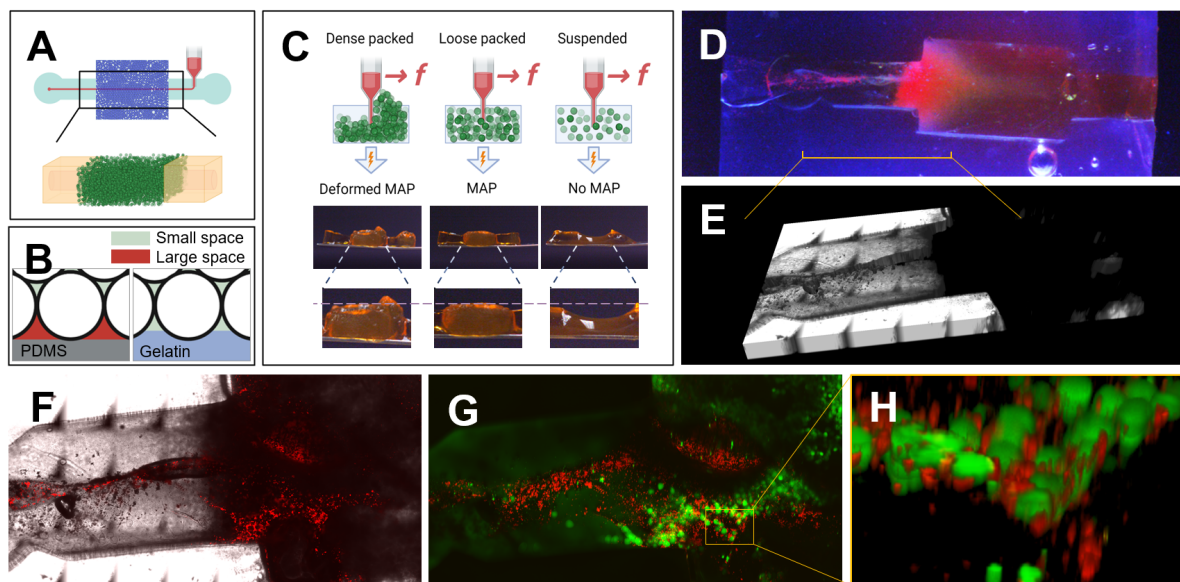


Figure 3.6: The creation and perfusion of an emb3D printed channel connected to an open MAP with a high-density capillary-like network. **(A)** Top: top-view schematic of printing (red) through liquid hydrogel (light blue) and microparticles (dark blue). Bottom: 3D schematic of solidified MAP in the middle (green) with perfusable channels on the side (orange). **(B)** Schematic featuring microgels (white), small void spaces (green), large void spaces (red), stiff PDMS bath (grey), and soft gelatin bath (blue) of how the stiffness of the bath affects the pore sizes on the edges of the MAP, and therefore also how it affects the path of least resistance during perfusion. **(C)** Schematic (top) and macroscopic images (bottom) of how microgel packing influences the self-healing and solidifying capacities of the bath. **(D)** Macroscopic image under UV light of a perfused structure embedded in gelatin. Perfusion was performed with red fluorescent particles. Yellow line indicates the location at which the next images (E-G) were taken in the construct. **(E)** Stitched 3D reconstruction of the region of interest with brightfield settings. The clear gelatin bath is more transparent than the bulk ATA holding the channel. Neither the microgels nor the perfused channels are transparent, and are therefore dark in this image. Because of the contrast, the bath, ATA hydrogel and channel are identifiable in this image. **(F)** Stitched 2D reconstruction combining brightfield (white) and perfusion particles (red) at the region of interest where it is observed that the particles go through the channel into the MAP. **(G)** Stitched 2D confocal image combining bulk ATA (dark green), microgels (bright green), and perfusion particles (red) where it is observed that the particles go through the channel into the MAP. **(H)** 3D confocal reconstruction in the perfused MAP where the perfusion particles (red) go around the microgels (green) through the capillary-like structure.

4

Discussion

The objective of this study was to engineer a perfusable and hierarchical vascular architecture using biocompatible materials. To realise this goal, first, a MAP from ATA microgels was manufactured with a high-density capillary-like network. Second, perfusable arteriole-like channels were fabricated using emb3D printing techniques. Third, a stable interface between the microgels and hydrogel was created using ATPS so that it was possible to fabricate a channel that was connected to the MAP. Last, the methods were combined to assemble a perfusable hierarchical porous network with micro- and macroscale vasculature (Fig. 1.1).

This chapter will present an in-depth analysis of the implications of the results obtained from the four experimental steps. Additionally, recommendations for future investigations will be proposed to advance the field of large-scale tissue engineering. In the last section, ideas and recommendations will be considered for future studies where cells are included in the structure.

Step 1: Microgel and MAP fabrication

The first step in this study involved the fabrication of monodisperse soft microgels using IAMF, which were then used to construct MAPs. We have established that the use of IAMF allows for high-throughput microgel fabrication, which is essential for scaling up tissue engineering. Although the microgels produced using IAMF are less spherical compared to those produced using conventional emulsion microfluidics, their shape can be improved with the nozzle positions of the IAMF device [34]. Furthermore, we hypothesise that the roundness is influenced by the deformation of the droplets in the air before and during crosslinking, which means that the roundness of the particles might be controlled by regulating the crosslinker flow rate.

We observe by eye that the microgels are soft and deformable after their first and before their second crosslinking step, which results in deformed microgels in the MAP. Although the shape and porosity of the MAP are dependent on the properties of the microgels resulting from the first crosslinking step, the stiffness of the MAP is formed during the second crosslinking step. During the second crosslinking step, not only the TA groups between various microgels will crosslink, but also TA groups within microgels internally, which will result in the stiffening of the microgels. This means that the stiffness of the microgels and the full MAP are separately tuneable and that the stiffness of the MAP is dependent on

photocrosslinker concentrations, photocrosslinking time, and the amount of TA on the Alg backbone. The range of microgel and MAP stiffness with ATA should be investigated by exposing the structures to compression tests.

In the future, various microgel shapes and sizes should be considered as the building blocks for MAPs. Previous research has demonstrated that the pore sizes within MAPs constructed from IAMF ATA microgels were similar and all in the capillary range for microgels of 50, 100, and 200 μm in size (unpublished). However, the underlying mechanism for this phenomenon remains unknown. We hypothesize that the stiffness and deformability of the microgels may have an impact on the pore sizes of the MAPs. Nevertheless, the void space fraction could differ due to the various sizes of the microgels. Also, the packing properties of Alg microgels of various sizes have not yet been explored. Polydispersity may lead to different particle packing and consequently affect the quality of void space in the MAPs, for example, the presence of smaller pore sizes. Apart from studying MAPs from variable spherical microgel sizes, it is also worth investigating the properties of MAPs constructed from non-spherical microgels in future studies. For example, researchers found that MAPs from randomly assembled rods have higher porosity and better cell ingrowth than MAPs from assembled spheres [67], [68]. Another example is that researchers have discovered that the shape of biological structures determines their functions, especially on the larger microscale, as that is the scale on which many biological functional units are organised. One example of those units is the elongated shape of striation in muscle bundles and bone osteons. Unlike spherical microgels, rod-shaped microgels can be collected and aligned, potentially resulting in more anatomically accurate microstructures. The shape of the microgel should be tailored to the structure of the target tissue.

Step 2: Emb3D printing perfusable channels in ATA

In the second step, the behaviour of ATA was studied regarding crosslinking variables and storage variables before fabricating perfusable arteriole-like channels in it. The liquid ATA bath was solidified using ruthenium (RU) and sodium persulfate (SPS) mediated photocrosslinking at $\lambda = 400\text{-}450$ nm. As visible light is used, colourless materials are preferred as they are less likely to interfere. We observe faster and stiffer photocrosslinking results with ATA_S than with ATA_A and ATA_B. The difference between those batches is that ATA_S has a higher degree of TA substitution, thus more TA groups that can form networks due to photocrosslinking. In future studies, this observation can be confirmed and quantified with compression tests.

We observe in both the swelling test and the printing test that larger channels are less stable than smaller channels. In the swelling test, the size of the hydrogel is not constricted. We observe that the size of the channel increases when the sample is exposed to MQ. We hypothesize that in this scenario, osmosis causes the gel to swell. As a result of this swelling, there is more space between the crosslinked polymer strands, which compromises the strength of the hydrogel and causes the material to tear. This can be solved by dissolving and storing the hydrogel sample in an isotonic solution so that there will be no net movement of water and therefore no swelling (or shrinking) will take place. On the other hand, in the printing test, the size of the hydrogel is constricted, which means that the larger the hole of the channel is, the less hydrogel there is on the side of the channel to stabilise it. We hypothesize that this causes larger printed channels to be unstable. This can be solved by increasing the size of the bath to make sure that there is enough remaining hydrogel on

the edges to stabilise the channel. However, upscaling the size of the bath is not infinitely possible, as there is a limitation to the depth to which the light can penetrate the sample, and therefore the depth at which photocrosslinking is effective, even when exposing the sample to light from multiple angles.

Our analysis revealed that channels generated by emb3D printing range from 300 to 500 μm in diameter. In the human body, the arterioles and arteries have a diameter ranging from 40 μm to 8 mm [20], [21]. This means that the size of the fabricated channels is within the range of existing vessels that they can be attached to for *in vivo* perfusion. Given that Alg is biocompatible and non-degradable in mammals [46], and TA-crosslinked gels have been reported to be stable *in vivo* [50], it is reasonable to assume that both the channel and MAP would remain stable after transplantation, allowing for the successful integration of the construct with the host tissue. Existing microvascular surgery methods include the use of sutures or adhesion agents. We acknowledge that further studies are required to investigate the stability of the channel and MAP *in vivo*, as well as which surgery method is most compatible with our ATA channels.

In the field of tissue engineering, researchers have proposed an alternative approach to our emb3D printed perfusable vessels, which involves embedding a perfusable fenestrated tube within engineered tissue [69]. Following their approach and applying it in our construct, we would build a MAP around a perfusable fenestrated tube. While this approach may seem simpler than emb3D printing channels in the early stages of large-scale tissue engineering, there are potential complications that arise from using a pre-made tube. For example, using a tube made of a different material may lead to the formation of fibrosis between the tube and the MAP. Additionally, the use of a pre-made tube restricts the flexibility of our freeform fabrication approach using emb3D printing. This flexibility is especially useful as we aim to mimic macroscale branched vascular networks. Therefore, while this proposed approach is an interesting alternative, we believe that our emb3D printing approach provides greater flexibility and potential for building more complex vascular networks.

Step 3: Stabilising the MAP-hydrogel interface with ATPS

In the third step, a stable interface was created through an ATPS between the MAP and the hydrogel where the materials were in contact with each other without interfering with each other's concentration and porous properties. In particular, we pre-saturated the microgels with polyethylene glycol (PEG-35K), which is a biocompatible polymer that is commonly used in various biomedical applications [70], [71]. The pre-saturation fulfils many functions. For one, it washes out the excess calcium in the microgel bath, making the microgels compatible to collect next to ATA hydrogel for the one-step fabrication protocol, rendering the previously conducted *manual print trials through DexTA* unnecessary (Appendix B). Furthermore, the pre-saturation and the ATPS also counteracted the dilution of the liquid ATA due to diffusion [46], [72] and the capillary forces exerted by the microgels on the liquid ATA [73], [74]. Furthermore, as will be elaborated on further, the pre-saturation has beneficial effects on the self-healing properties of the microgel bath.

To distinguish between the two colourless liquids for ATPS stability studies, a visualisation method was invented based on the refractive indexes of the polymers. Refractive indexes are a measure of how much a material bends light as it passes through it, which is dependent on the chemical properties and concentration of the polymer [62]. As the two

polymeric solutions have different chemical properties and concentrations, they also have different refractive indexes [63]–[65]. To distinguish between the two colourless liquids for ATPS stability studies, the interface could be visualised by looking at the shadow.

We observed lower ATPS stability when the polymers were dissolved in PBS than in MQ. This was an unexpected observation, as our initial hypothesis was that the salts in the PBS would stabilise the ATPS, as it is known that polymer-salt ATPS exists next to polymer-polymer ATPS [75], [76]. Even though the limited stability in the PBS system was sufficient for this study, methods to stabilise the interface further are beneficial for future studies, especially with upscaled tissue engineering in mind, where it is highly likely that more channels will need to be fabricated and therefore a longer window of stability will be needed. We hypothesise that the ATPS stability can be increased by using a solution with a higher PEG-35K concentration.

To create a connected structure, the right balance between the microgel pre-saturation and the amount of hydrogel was needed. When the microgels are not saturated enough, the hydrogel would penetrate the microgel structure due to capillary forces. On the other hand, if the microgels are oversaturated, the hydrogel would not have sufficient contact with the microgels for photocrosslinking on the interface. In the case of oversaturation, we found that the hydrogel could be brought in contact with the microgels anyways by adding a larger volume of hydrogel, effectively increasing the pressure on the hydrogel in the direction of the microgels. However, we found that creating such an overfull structure was not beneficial for channel fabrication, as channel fabrication requires depositing more material into the structure, which can cause the print bath to overflow.

After photocrosslinking, we observe a clear and connected interface between the MAP and the ATA. We assume that when this structure is fabricated with the presence of a printed channel, the structure will still be connected, and therefore, we hope that there is no leakage of perfusion fluid between the channel and the MAP. However, we predict that the interface might be less stable with the presence of a hollow perfusable channel, as its presence will reduce the contact area between the MAP and the channel, and therefore the amount of photocrosslinked TA connections. Therefore, we hypothesise that the interface may need further stabilisation, especially in situations where forces are exerted on the interface, such as for perfusion and *in vivo* transplantation, as in both scenarios, the forces from the fluid flow will act perpendicular on the interface surfaces. Our proposed solution to stabilise the interface is to put the whole construct in a holder so that the internal structures and interfaces are supported.

Step 4: Creating perfusable hierarchical vasculature

In the fourth and final step of this study, the appropriate microgel pre-saturation was determined for emb3D printing and MAP formation and the final hierarchically vascular and perfusable construct was created combining by combining approaches from the previous three steps. In this step, we exploited the self-healing properties of the microgel bath during emb3D printing [54]–[58], which had to be investigated in combination with microgel presaturation. The presaturation and therefore packing of the microgels is a crucial factor that influences the formation and the shape of the MAP. If the microgels are densely packed, the bath loses its self-healing properties [77]. Conversely, if the microgels are too loosely suspended, their surfaces do not make contact with each other, leading to insufficient crosslinking between the microgels. Therefore, it was essential to control the microgel

packing by adjusting the amount of pre-saturation in the microgel bath.

Other researchers have previously leveraged the self-healing and supportive characteristics of microgel baths for freeform printing, as reported in the literature [58], [78], [79]. For instance, a microgel bath can be utilised to print an anatomically precise heart model [80]. Moreover, printing sacrificial channels in microgel baths is not a new concept [23], [81], [82]. Nonetheless, these researchers fabricated their channels in densely packed microgel baths, where the porous structure of MAPs was relinquished in favour of enhanced stability and support for the printed structure. Consequently, these researchers only perfused the printed structure, and they did not perfuse a microporous bath as we did in our study.

Another proposed approach to fabricate perfusable macroscale vessels involves emb3D printing a solid tubular network through the MAP-and-liquid-hydrogel structure, followed by sacrificing the solid ink once the MAP and bulk hydrogel are formed. This approach overcomes the challenge of maintaining the stability and connectivity of the liquid ink for a longer period, especially near the ATPS interface. Solidifying the ink in between can be particularly advantageous when fabricating larger perfusable channels in larger structures, where the separation between the liquid ink, liquid hydrogel, and ATPS interface needs to exist for an extended period before the liquid hydrogel solidifies. Despite the advantages of this approach, we acknowledge that solidified inks, for instance, gelatin, in constructs can be challenging to wash out. However, other researchers have successfully printed and sacrificed gelatin inks in microgel baths [81], demonstrating the feasibility of this approach.

Initially, we elected to fabricate the print baths from PDMS, which is a widely used silicone elastomer with beneficial properties such as gas permeability, flexibility, elasticity, and biocompatibility [83]. However, when perfusing the MAP through the channel, it was observed that the particles in the perfusion fluid preferred to traverse the bath from the side of the MAP instead of through the MAP. We have two hypotheses that can explain this phenomenon. First, we hypothesised that the spaces on the side of the MAP were larger than the pores in the MAP due to higher PDMS stiffness than MAP stiffness, which made the resistance on the side of the MAP lower and therefore the preferred path of the perfusion particles. Second, we thought that the presence of that particular path of least resistance could be attributed to the hydrophobic properties of PDMS [83] which rejects friction with the microgels.

To maintain perfusion throughout the MAP, we proposed to minimise the size of the pores at the edges and to increase the friction between the bath and the microgels. We achieved this successfully by using a softer and hydrophilic material to fabricate the perfusable structure in, namely as 10% w/v gelatin. Gelatin is a naturally occurring biopolymer derived from collagen, which has been widely studied and is known to be biocompatible with low immunogenicity [84]–[87].

In the macroscopic UV image of the perfused construct (Fig. 3.6E), we observed that the fluorescent perfusion particles are mainly visible at the beginning of the construct. We hypothesise that this is due to the larger particles becoming trapped within the pores. Based on our knowledge that the fluorescent particles were strained to a diameter of up to 70 μm and that the pores have an average diameter of 61.17 μm , this hypothesis is highly plausible. To further support this claim, we can also observe a faint fluorescent line extending towards the outlet in the same image. Additionally, during the experiment, we observed fluid exiting the outlet, indicating successful perfusion through the MAP despite incomplete traversal of the larger fluorescent particles. However, to support this claim and to fur-

ther study the behaviour of perfusion flow through the capillary-like MAP, perfusion should be performed with red blood cell (RBC)-sized particles of 7-8 μm [88], [89]. Ideally, this flow study with RBC-sized particles should be conducted at a realistic flow rate in the capillaries, which is about 0.5 to 1.5 mm/sec in human capillaries [90], to gain insights on the number of inlets needed to fully saturate any MAP volume through perfusion.

In our study, we have observed that particles in the perfusion fluid may settle at the bottom of the construct due to gravitational forces when perfusing in the horizontal plane. We predict that it can become a challenge to fully perfuse and saturate a larger MAP when the perfusion direction is horizontal, therefore, we propose to either keep the MAP volumes small or to perfuse the larger MAP in the same direction as the gravitational forces and taking advantage of the gravitational forces for more effective perfusion in future studies. However, both approaches require further investigation.

Another consideration is the limited depth of our laser scanning confocal microscope, which may not be sufficient for analysing larger and deeper constructs. Thus, alternative methods for visualization and analysis should be explored for larger perfused constructs. One option for visualising and analysing large constructs that are too deep for confocal microscopy is to use optical coherence tomography (OCT), which uses light waves to create high-resolution, cross-sectional images. OCT has a depth of focus of approximately 700 μm , which is a deeper penetration depth than confocal microscopy [91]. OCT can be used to visualise the internal structures of large constructs in a non-invasive manner at a resolution of 20-5 μm [91].

Although engineering perfusable capillary-like networks is a significant breakthrough, scaling up the size of the constructs presents several challenges. One major limitation of photocrosslinking is the depth of light penetration into the hydrogel, which restricts the size of photocrosslinked constructs. To overcome this limitation, we propose two approaches. The first approach involves activating TA crosslinking with HRP and H_2O_2 , as an alternative to photocrosslinking ATA. However, this method results in weak links due to the low degree of TA substitution on ATA, as observed in preliminary studies. To address this issue, we could increase the degree of TA substitution on our ATA, or use a different hydrogel with more (substituted) TA groups. The second approach involves building a full construct layer-by-layer within the penetration depth of the light, which could result in variations in properties and weak connections between the layers. A third potential approach is to make several small constructs and stack them together to form a larger construct. While these approaches present challenges, they provide potential solutions to overcome the limitations of photocrosslinking and enable the engineering of larger tissue constructs. To scale up the fabrication of tissue, it is essential to determine the arteriole density required for full perfusion of the MAP. While previous studies have provided estimates for arteriole density, these values can be influenced by material properties, such as frictional resistance caused by Alg in both the channel and MAP. Therefore, to determine the optimal channel diameter and quantity for full perfusion of our MAP structure, we propose using simulation to precisely calculate the required arteriole density. Additionally, simulation can provide insight into the stability of the channels and MAP for varying perfusion flow rates, including the impact of branching on pressure changes along the channels. It should be noted that while our current design includes only one inlet and outlet tube, the addition of more branches during printing may result in changes in pressure that could potentially be leveraged for large-scale tissue engineering. Further investigation into this phenomenon is warranted.

To prevent leakage during perfusion and facilitate transplantation, it would be advantageous to utilise a holder to contain the tissue construct. Gelatin, as used in our experiments as a print bath, is a suitable biocompatible option, but it has the disadvantage of melting at mammalian *in vivo* temperatures. To address this issue, GelMA, which is a variant of gelatin that remains solid, could be used [92], [93]. By encapsulating the engineered tissue within such a bath, a protective barrier could be formed between the construct and native tissue, which can become a permanent barrier over time through the process of fibrosis.

Including living cells to the hierarchical vascular structure

In conventional tissue engineering techniques, making large, clinically relevant-sized constructs using cell encapsulation and seeding methods is limited. This is because the formation of the tissue depends on cell migration and growth into the scaffold, which is a time-consuming process [94]. Alternatively, encapsulating cells in a bulk hydrogel results in a necrotic core due to the limited diffusion of oxygen and nutrients [25], [26].

To render our system compatible with cell culture, it is imperative to dissolve all samples in materials that are suitable for this purpose. Alg, when dissolved in culture medium or PBS, has been shown to be challenging to sterilise in previous studies, however, we have successfully sterilised Alg solutions in HEPES buffered saline [35]. Therefore, we propose to dissolve and sterilise our ATA in HEPES buffered saline for this purpose as well. Subsequently, we suggest performing new channel swelling studies and ATPS stability experiments with these new materials. Once the structure is constructed using these materials, it should ideally be maintained in a culture medium, as we intend to introduce cells to the system. However, if we find that the swelling and ATPS stability are comparable in other alternatives, such as PBS, we can use them for research purposes, similar to how we replaced the culture medium with PBS in this study. To study the effect of continuous perfusion flow on the structure, a perfusion bioreactor can be used.

Our construct is designed for the addition of cells, where tissue cells are intended to be encapsulated in the microgels, forming microtissues. From previous studies, it has been established that various cell types such as HepG2, MIN6, and MSCs can be successfully encapsulated in microgels using IAMF [34], [35]. As these microtissues can be fabricated within the diffusion limit, we hypothesise that we can use those microtissues to make large living MAPs without necrotic cores, which is a crucial step towards large-scale tissue engineering. Therefore, it is highly important to test this hypothesis and to achieve maintained cell viability in MAPs. One of the expected challenges is weighing the MAP strength induced by photocrosslinking against cell viability, as it is known that high concentrations of the photocrosslinker SPS both increases photocrosslinking quality and is toxic to cells in high quantity. Potential possibilities to enhance the performance of cells by incorporating growth factors or other beneficial materials in the hydrogel can be explored. Additionally, anti-inflammatory agents or other drugs could be incorporated to improve cell behaviour. For our experimental setup, it is also necessary to study the cell response to emb3D printing through a living modular bath in which cells are encapsulated (Fig. 4.1). The advantage of this setup is that the cells are encapsulated and thus protected. However, cell response must still be studied, especially for more fragile cell types.

To functionalise the vessels in the engineered tissues, we aim to seed human umbilical vein endothelial cells (HUVECs) onto the MAP and the channels for vessel formation in future studies. The presence of HUVECs is essential for regulating the exchange of substances

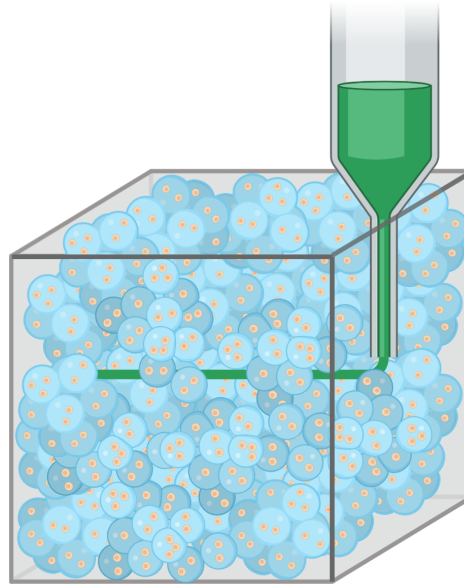


Figure 4.1: Schematic of emb3D printing through a microtissue bath. Schematic created with BioRender.

between the blood and surrounding tissues. To enhance HUVEC adhesion to the scaffold, a collagen coating can be applied to the Alg channels. Previous studies have demonstrated successful cell ingrowth within a MAP scaffold [32] and effective cell adhesion to collagen-coated hydrogel channels [82], thus supporting the feasibility of this approach. The ability to encapsulate various cell types in distinct microgels presents an opportunity to produce a living structure with heterogeneity. In theory, the injectability of microgels provides control over the positioning of different microtissues within a single construct, allowing for the creation of a heterogeneous patterned living structure. As native tissues and organs in the human body are composed of different types of cells, it would be remarkable to fabricate such a large living heterogeneous structure. The next step would be to investigate how emb3D printing movements affect the individual positions of microgels. If we could predict and control the placement of individual microtissues, we could fabricate macroscale channels in the patterned heterogeneous microtissue bath.

The research enables the development of large cell-laden constructs with sufficient vasculature within the diffusion limit for all cells, thereby avoiding necrotic cores. We hope that our technique will advance the field of tissue engineering, enabling the generation of larger and more complex tissue constructs.

Tissue engineering has the potential to revolutionise medical treatment and provide solutions to various health problems. However, it also raises ethical concerns that need to be addressed before clinical applications can be considered. One concern is the use of human embryonic stem cells or fetal tissues, which raises ethical and legal issues surrounding their sourcing and usage. Additionally, there are concerns about the safety and efficacy of engineered tissues, as well as the possibility of unintended consequences such as unforeseen immune responses or tumorigenesis. There are also questions about the accessibility and affordability of these treatments and potential inequalities in access to cutting-edge therapies. As such, ethical considerations need to be carefully considered and addressed in the development and deployment of tissue engineering technologies for clinical applications. So far, there is no ethical guidance for engineered tissues in clinical trials [95].

5

Conclusion

The goal of this study was to fabricate a structure with hierarchical vasculature, in particular, a microporous capillary-like network and macroscale perfusable channels. In this study, we created a MAP that exhibits a microscale capillary-like interconnected porous network that is inherent in its structure. The MAP was built from monodisperse ATA microgels, which were fabricated through IAMF. IAMF was found to be about 250 times faster than conventional emulsion microfluidics, making high-throughput microgel and micro-tissue fabrication possible.

We have successfully performed emb3D printing to fabricate perfusable macroscale channels in ATA hydrogel. Our results demonstrate that the hydrogel can be solidified through photocrosslinking within a feasible timeframe while maintaining the hollow and perfusable nature of the printed channel. Moreover, we have observed that dissolving and storing ATA in cell culture-compatible materials, such as PBS or culture medium, does not adversely affect the size and stability of the channel for up to a week. We found that the channel size fabricated by emb3D printing was dependent on two printing parameters: larger infuse rates ($i[\mu\text{L}/\text{min}]$) and lower print speeds ($f[\text{mm}/\text{min}]$) would cause the channel size to increase. After careful consideration, we decided to fabricate perfusable channels with a diameter of approximately 0.5 mm with the i50f100 settings as a proof of concept.

We have also achieved successful exclusion of the ATA hydrogel from the MAP by pre-saturating the microgels with a biocompatible polymeric solution consisting of 5% w/v PEG-35K in PEG that forms an ATPS with the 1 % w/v ATA in PEG hydrogel. Simultaneously, the pre-saturation allowed for the formation of a connected structure between the MAP and the bulk hydrogel and it enabled the self-healing abilities of the microgel bath. Furthermore, we have demonstrated the simultaneous fabrication of the MAP and perfusable channels through photocrosslinking. The proof-of-concept perfusion experiment showed that perfusion of the MAP through the printed channel was successful when encapsulated in a gelatin bath. This innovative approach represents a significant advancement in the field of tissue engineering, as it has not been previously demonstrated to engineer a multi-scale vascular tree in this manner. We believe that this novel approach has the potential to overcome the current limitations in large-scale tissue engineering by enabling the creation of hierarchical vascular structures in living tissues.

Acknowledgements

The author would like to express her gratitude to Maik Schot, Malin Becker, and Dr. Jeroen Leijten from the Developmental BioEngineering group at the University of Twente for their invaluable guidance and support throughout this research project. In particular, the author would like to express her gratitude to Maik R. Schot, who provided extensive training on microgel-related topics. He also contributed to the calibration curve for the nanodrop analysis, created the mould for MAP formation, and wrote the Matlab script for MAP analysis. Also, the author would like to express her thanks to Malin L. Becker, who provided invaluable expertise on chemistry and emb3D printing. She also kindly provided the DexTA, helped design the ATPS analysis setup, and created bubble graphs in Origin Pro. Maik Schot and Malin Becker assisted with macroscopic and microscopic confocal imaging, respectively. The author appreciates the collaborative and supportive environment created by the members of the Developmental BioEngineering group, which made this research project possible. The author also extends her appreciation to Dr. Lidy Fratila-Apachitei, Dr. Jie Zhou, and Dr. Amir Zadpoor from the Technical University of Delft for their supervision and contribution to the graduation committee. Finally, the author thanks Yida Tao for her contribution to the cover page of this thesis.

Disclosure Statement

No competing financial interests exist.

References

- [1] WHO, “Human organ and tissue transplantation - Report by the Director-General,” in *World Health Assembly*, vol. 75, 2022, p. 7.
- [2] ONT, WHO, and WBMT, *Global Observatory on Donation and Transplantation*, 2021. [Online]. Available: www.transplant-observatory.org.
- [3] HRSA, *Organ Donation Statistics*, 2022. [Online]. Available: <https://www.organdonor.gov/learn/organ-donation-statistics>.
- [4] C. Mandrycky, Z. Wang, K. Kim, and D. H. Kim, “3D bioprinting for engineering complex tissues,” *Biotechnology Advances*, vol. 34, no. 4, pp. 422–434, 2016, ISSN: 07349750. DOI: 10.1016/j.biotechadv.2015.12.011. [Online]. Available: <http://dx.doi.org/10.1016/j.biotechadv.2015.12.011>.
- [5] N. A. Kurniawan, “The ins and outs of engineering functional tissues and organs: Evaluating the in-vitro and in-situ processes,” *Current Opinion in Organ Transplantation*, vol. 24, no. 5, pp. 590–597, Oct. 2019, ISSN: 15317013. DOI: 10.1097/MOT.0000000000000690. [Online]. Available: https://www.researchgate.net/publication/335005047_The_ins_and_outs_of_engineering_functional_tissues_and_organ_evaluating_the_in-vitro_and_in-situ_processes.
- [6] S. Sohn, M. Van Buskirk, M. J. Buckenmeyer, R. Londono, and D. Faulk, “Whole Organ Engineering: Approaches, Challenges, and Future Directions,” *Applied Sciences 2020, Vol. 10, Page 4277*, vol. 10, no. 12, p. 4277, Jun. 2020, ISSN: 2076-3417. DOI: 10.3390/AP10124277. [Online]. Available: <https://www.mdpi.com/2076-3417/10/12/4277/htm><https://www.mdpi.com/2076-3417/10/12/4277>.
- [7] A. F. Pellegata, A. M. Tedeschi, and P. De Coppi, “Whole organ tissue vascularization: Engineering the tree to develop the fruits,” *Frontiers in Bioengineering and Biotechnology*, vol. 6, no. MAY, p. 56, May 2018, ISSN: 22964185. DOI: 10.3389/FBIOE.2018.00056/BIBTEX.
- [8] A. Petrosyan, F. Montali, A. Peloso, *et al.*, “Regenerative medicine technologies applied to transplant medicine. An update,” *Frontiers in Bioengineering and Biotechnology*, vol. 10, no. September, pp. 1–18, 2022, ISSN: 22964185. DOI: 10.3389/fbioe.2022.1015628.
- [9] I. Marei, T. Abu Samaan, M. A. Al-Quradaghi, A. A. Farah, S. H. Mahmud, H. Ding, and C. R. Triggler, “3D Tissue-Engineered Vascular Drug Screening Platforms: Promise and Considerations,” *Frontiers in cardiovascular medicine*, vol. 9, Mar. 2022, ISSN: 2297-055X. DOI: 10.3389/FCVM.2022.847554. [Online]. Available: <https://pubmed.ncbi.nlm.nih.gov/35310996/>.

- [10] A. S. Khalil, R. Jaenisch, and D. J. Mooney, "Engineered tissues and strategies to overcome challenges in drug development," *Advanced Drug Delivery Reviews*, vol. 158, p. 116, Jan. 2020, ISSN: 18728294. DOI: 10.1016/J.ADDR.2020.09.012. [Online]. Available: [/pmc/articles/PMC7518978/%20/pmc/articles/PMC7518978/?report=abstract%20https://www.ncbi.nlm.nih.gov/pmc/articles/PMC7518978/](https://pubmed.ncbi.nlm.nih.gov/34299132/).
- [11] L. S. Neves, M. T. Rodrigues, R. L. Reis, and M. E. Gomes, "Current approaches and future perspectives on strategies for the development of personalized tissue engineering therapies," [http://dx.doi.org/10.1080/23808993.2016.1140004](https://doi.org/10.1080/23808993.2016.1140004), vol. 1, no. 1, pp. 93–108, Jan. 2016, ISSN: 23808993. DOI: 10.1080/23808993.2016.1140004. [Online]. Available: <https://www.tandfonline.com/doi/abs/10.1080/23808993.2016.1140004>.
- [12] B. A. Aguado, J. C. Grim, A. M. Rosales, J. J. Watson-Capps, and K. S. Anseth, "Engineering precision biomaterials for personalized medicine," *Science translational medicine*, vol. 10, no. 424, Jan. 2018, ISSN: 19466242. DOI: 10.1126/SCITRANSLMED.AAM8645. [Online]. Available: [/pmc/articles/PMC6079507/%20/pmc/articles/PMC6079507/?report=abstract%20https://www.ncbi.nlm.nih.gov/pmc/articles/PMC6079507/](https://pubmed.ncbi.nlm.nih.gov/34299132/).
- [13] I. M. Tayler and R. S. Stowers, "Engineering hydrogels for personalized disease modeling and regenerative medicine," *Acta Biomaterialia*, vol. 132, pp. 4–22, Sep. 2021, ISSN: 1742-7061. DOI: 10.1016/J.ACTBIO.2021.04.020.
- [14] T. Ben-Arye and S. Levenberg, "Tissue Engineering for Clean Meat Production," *Frontiers in Sustainable Food Systems*, vol. 3, p. 46, Jun. 2019, ISSN: 2571581X. DOI: 10.3389/FSUFS.2019.00046/BIBTEX.
- [15] D. H. Kang, F. Louis, H. Liu, H. Shimoda, Y. Nishiyama, H. Nozawa, M. Kakitani, D. Takagi, D. Kasa, E. Nagamori, S. Irie, S. Kitano, and M. Matsusaki, "Engineered whole cut meat-like tissue by the assembly of cell fibers using tendon-gel integrated bio-printing," *Nature Communications* 2021 12:1, vol. 12, no. 1, pp. 1–12, Aug. 2021, ISSN: 2041-1723. DOI: 10.1038/s41467-021-25236-9. [Online]. Available: <https://www.nature.com/articles/s41467-021-25236-9>.
- [16] J. Reiss, S. Robertson, and M. Suzuki, "Cell Sources for Cultivated Meat: Applications and Considerations throughout the Production Workflow," *International journal of molecular sciences*, vol. 22, no. 14, Jul. 2021, ISSN: 1422-0067. DOI: 10.3390/IJMS22147513. [Online]. Available: <https://pubmed.ncbi.nlm.nih.gov/34299132/>.
- [17] M. S. Arshad, M. Javed, M. Sohaib, F. Saeed, A. Imran, and Z. Amjad, "Tissue engineering approaches to develop cultured meat from cells: A mini review," *Cogent Food & Agriculture*, vol. 3, no. 1, p. 1320814, 2017, ISSN: 23311932. DOI: 10.1080/23311932.2017.1320814. [Online]. Available: <https://www.tandfonline.com/doi/abs/10.1080/23311932.2017.1320814>.
- [18] M. Hofer and M. P. Lutolf, "Engineering organoids," *Nature Reviews Materials* 2021 6:5, vol. 6, no. 5, pp. 402–420, Feb. 2021, ISSN: 2058-8437. DOI: 10.1038/s41578-021-00279-y. [Online]. Available: <https://www.nature.com/articles/s41578-021-00279-y>.

- [19] Z. Zhao, X. Chen, A. M. Dowbaj, A. Sljukic, K. Bratlie, L. Lin, E. L. S. Fong, G. M. Balachander, Z. Chen, A. Soragni, M. Huch, Y. A. Zeng, Q. Wang, and H. Yu, "Organoids," *Nature Reviews Methods Primers* 2022 2:1, vol. 2, no. 1, pp. 1–21, Dec. 2022, ISSN: 2662-8449. DOI: 10.1038/s43586-022-00174-y. [Online]. Available: <https://www.nature.com/articles/s43586-022-00174-y>.
- [20] M. A. Traore and S. C. George, *Tissue Engineering the Vascular Tree*, Dec. 2017. DOI: 10.1089/ten.teb.2017.0010.
- [21] M. Peckham, *Capillaries*, 2003. [Online]. Available: <https://www.histology.leeds.ac.uk/circulatory/capillaries.php>.
- [22] X. Zeng, Z. Meng, J. He, M. Mao, X. Li, P. Chen, J. Fan, and D. Li, "Embedded bioprinting for designer 3D tissue constructs with complex structural organization," *Acta Biomaterialia*, vol. 140, pp. 1–22, 2022, ISSN: 18787568. DOI: 10.1016/j.actbio.2021.11.048.
- [23] M. A. Skylar-Scott, S. G. Uzel, L. L. Nam, J. H. Ahrens, R. L. Truby, S. Damaraju, and J. A. Lewis, "Biomufacturing of organ-specific tissues with high cellular density and embedded vascular channels," *Science Advances*, vol. 5, no. 9, Sep. 2019, ISSN: 23752548. DOI: 10.1126/SCIADV.AAW2459. [Online]. Available: [/pmc/articles/PMC6731072/](https://www.ncbi.nlm.nih.gov/pmc/articles/PMC6731072/) <https://www.ncbi.nlm.nih.gov/pmc/articles/PMC6731072/?report=abstract> <https://www.ncbi.nlm.nih.gov/pmc/articles/PMC6731072/>.
- [24] S. Fleischer, D. N. Tavakol, and G. Vunjak-Novakovic, "From arteries to capillaries: approaches to engineering human vasculature," *Advanced functional materials*, vol. 30, no. 37, Sep. 2020, ISSN: 16163028. DOI: 10.1002/ADFM.201910811. [Online]. Available: [/pmc/articles/PMC7942836/](https://www.ncbi.nlm.nih.gov/pmc/articles/PMC7942836/) [/pmc/articles/PMC7942836/?report=abstract](https://www.ncbi.nlm.nih.gov/pmc/articles/PMC7942836/?report=abstract) <https://www.ncbi.nlm.nih.gov/pmc/articles/PMC7942836/>.
- [25] S. Grebenyuk, A. R. Abdel Fattah, M. Kumar, B. Toprakhisar, G. Rustandi, A. Vananroye, I. Salmon, C. Verfaillie, M. Grillo, and A. Ranga, "Large-scale perfused tissues via synthetic 3D soft microfluidics," *Nature Communications* 2023 14:1, vol. 14, no. 1, pp. 1–18, Jan. 2023, ISSN: 2041-1723. DOI: 10.1038/s41467-022-35619-1. [Online]. Available: <https://www.nature.com/articles/s41467-022-35619-1>.
- [26] S. Grebenyuk and A. Ranga, "Engineering organoid vascularization," *Frontiers in Bioengineering and Biotechnology*, vol. 7, no. MAR, p. 39, Mar. 2019, ISSN: 22964185. DOI: 10.3389/FBIOE.2019.00039/BIBTEX.
- [27] J. M. de Rutte, J. Koh, and D. Di Carlo, "Scalable High-Throughput Production of Modular Microgels for In Situ Assembly of Microporous Tissue Scaffolds," *Advanced Functional Materials*, vol. 29, no. 25, pp. 1–10, 2019, ISSN: 16163028. DOI: 10.1002/adfm.201900071.
- [28] L. Riley, P. Cheng, and T. Segura, "Void space and scaffold analysis of packed particles: applications in granular biomaterials," 2022.
- [29] N. F. Truong, E. Kurt, N. Tahmizyan, S. C. Lesher-Pérez, M. Chen, N. J. Darling, W. Xi, and T. Segura, "Microporous annealed particle hydrogel stiffness, void space size, and adhesion properties impact cell proliferation, cell spreading, and gene transfer," *Acta Biomaterialia*, vol. 94, pp. 160–172, 2019, ISSN: 18787568. DOI: 10.1016/j.actbio.2019.02.054. [Online]. Available: <https://doi.org/10.1016/j.actbio.2019.02.054>.

- [30] A. Isaac, F. Jivan, S. Xin, J. Hardin, X. Luan, M. Pandya, T. G. Diekwisch, and D. L. Alge, "Microporous Bio-orthogonally Annealed Particle Hydrogels for Tissue Engineering and Regenerative Medicine," *ACS Biomaterials Science and Engineering*, vol. 5, no. 12, pp. 6395–6404, Dec. 2019, ISSN: 23739878. DOI: 10.1021/ACSBIOMATERIALS.9B01205/ASSET/IMAGES/LARGE/AB9B01205{_}0006.JPEG. [Online]. Available: <https://pubs.acs.org/doi/full/10.1021/acsbiomaterials.9b01205>.
- [31] A. E. Widener, M. Bhatta, T. E. Angelini, and E. A. Phelps, "Guest-host interlinked PEG-MAL granular hydrogels as an engineered cellular microenvironment," *Biomaterials Science*, vol. 9, no. 7, pp. 2480–2493, 2021, ISSN: 20474849. DOI: 10.1039/d0bm01499k.
- [32] D. R. Griffin, W. M. Weaver, P. O. Scumpia, D. Di Carlo, and T. Segura, "Accelerated wound healing by injectable microporous gel scaffolds assembled from annealed building blocks," *Nature Materials*, vol. 14, no. 7, pp. 737–744, 2015, ISSN: 14764660. DOI: 10.1038/nmat4294.
- [33] D. R. Griffin, M. M. Archang, C. H. Kuan, W. M. Weaver, J. S. Weinstein, A. C. Feng, A. Ruccia, E. Sideris, V. Ragkousis, J. Koh, M. V. Plikus, D. Di Carlo, T. Segura, and P. O. Scumpia, "Activating an adaptive immune response from a hydrogel scaffold imparts regenerative wound healing," *Nature Materials*, vol. 20, no. 4, pp. 560–569, 2021, ISSN: 14764660. DOI: 10.1038/s41563-020-00844-w. [Online]. Available: <http://dx.doi.org/10.1038/s41563-020-00844-w>.
- [34] C. W. Visser, T. Kamperman, L. P. Karbaat, D. Lohse, and M. Karperien, "In-air microfluidics enables rapid fabrication of emulsions, suspensions, and 3D modular (bio)materials," *Science Advances*, vol. 4, no. 1, 2018, ISSN: 23752548. DOI: 10.1126/sciadv.aao1175.
- [35] L. Y. Tao, "Ultra-high throughput production of annealable microtissues to engineer perfusable tissues due to capillary-like networks," Technical University of Delft, Delft, Tech. Rep., 2022, p. 7.
- [36] M. Schot, N. Araújo-gomes, B. V. Loo, T. Kamperman, and J. Leijten, "Bioactive Materials Scalable fabrication, compartmentalization and applications of living microtissues," *Bioactive Materials*, vol. 19, no. April 2022, pp. 392–405, 2023, ISSN: 2452-199X. DOI: 10.1016/j.bioactmat.2022.04.005. [Online]. Available: <https://doi.org/10.1016/j.bioactmat.2022.04.005>.
- [37] P. V. Blokzijl, "Bottom-up Tissue Engineering of Immunoprotected Insulin-Producing Microtissues to Improve Islet Cell Transplantation for," University of Enschede, Enschede, Tech. Rep., 2022, p. 30.
- [38] M. Dalheim, J. Vanacker, M. A. Najmi, F. L. Aachmann, B. L. Strand, and B. E. Christensen, "Efficient functionalization of alginate biomaterials," *Biomaterials*, vol. 80, pp. 146–156, Feb. 2016, ISSN: 1878-5905. DOI: 10.1016/J.BIOMATERIALS.2015.11.043. [Online]. Available: <https://pubmed.ncbi.nlm.nih.gov/26708091/>.

- [39] J. D. Medina, M. Alexander, M. D. Hunckler, M. A. Fernández-Yagüe, M. M. Coronel, A. M. Smink, J. R. Lakey, P. de Vos, A. J. García, J. D. Medina Biomedical Engineering, M. Alexander, M. D. Hunckler, M. A. Fernández-Yagüe, M. M. Coronel, A. J. García, A. M. Smink, P. de Vos, and J. R. Lakey, "Functionalization of Alginate with Extracellular Matrix Peptides Enhances Viability and Function of Encapsulated Porcine Islets," *Advanced Healthcare Materials*, vol. 9, no. 9, p. 2000102, May 2020, ISSN: 2192-2659. DOI: 10.1002/ADHM.202000102. [Online]. Available: <https://onlinelibrary.wiley.com/doi/full/10.1002/adhm.202000102><https://onlinelibrary.wiley.com/doi/abs/10.1002/adhm.202000102><https://onlinelibrary.wiley.com/doi/10.1002/adhm.202000102>.
- [40] S. D. Kim, S. Jin, S. Kim, D. Son, and M. Shin, "Tyramine-Functionalized Alginate-Collagen Hybrid Hydrogel Inks for 3D-Bioprinting," *Polymers*, vol. 14, no. 15, Aug. 2022, ISSN: 2073-4360. DOI: 10.3390/POLYM14153173. [Online]. Available: <https://pubmed.ncbi.nlm.nih.gov/35956690/>.
- [41] J. Hou, C. Li, Y. Guan, Y. Zhang, and X. X. Zhu, "Enzymatically crosslinked alginate hydrogels with improved adhesion properties," *Polymer Chemistry*, vol. 6, no. 12, pp. 2204–2213, Mar. 2015, ISSN: 1759-9962. DOI: 10.1039/C4PY01757A. [Online]. Available: <https://pubs.rsc.org/en/content/articlehtml/2015/py/c4py01757a><https://pubs.rsc.org/en/content/articlelanding/2015/py/c4py01757a>.
- [42] A. Schulz, M. M. Gepp, F. Stracke, H. von Briesen, J. C. Neubauer, and H. Zimmermann, "Tyramine-conjugated alginate hydrogels as a platform for bioactive scaffolds," *Journal of Biomedical Materials Research - Part A*, vol. 107, no. 1, pp. 114–121, Jan. 2019, ISSN: 15524965. DOI: 10.1002/JBM.A.36538. [Online]. Available: https://www.researchgate.net/publication/327897602_Tyramine-conjugated_alginate_hydrogels_as_a_platform_for_bioactive_scaffolds_TYRAMINE-CONJUGATED_ALGINATE_HYDROGELS.
- [43] M. I. Neves, L. Moroni, and C. C. Barrias, "Modulating Alginate Hydrogels for Improved Biological Performance as Cellular 3D Microenvironments," *Frontiers in Bioengineering and Biotechnology*, vol. 8, p. 665, Jun. 2020, ISSN: 22964185. DOI: 10.3389/FBIOE.2020.00665/BIBTEX.
- [44] R. V. Balaj, S. W. Cho, P. Singh, and L. D. Zarzar, "Supporting Information Polyelectrolyte hydrogel capsules as stabilizers for reconfigurable complex emulsions Electronic Supplementary Material (ESI) for," 2019.
- [45] Y. Hori, A. M. Winans, and D. J. Irvine, "Modular Injectable Matrices Based on Alginate Solution/Microsphere Mixtures That Gel in situ and Co-Deliver Immunomodulatory Factors," *Acta biomaterialia*, vol. 5, no. 4, p. 969, 2009, ISSN: 17427061. DOI: 10.1016/J.ACTBIO.2008.11.019. [Online]. Available: <https://pubmed.ncbi.nlm.nih.gov/pmc/articles/PMC3042245/><https://pubmed.ncbi.nlm.nih.gov/pmc/articles/PMC3042245/?report=abstract><https://www.ncbi.nlm.nih.gov/pmc/articles/PMC3042245/>.
- [46] K. Y. Lee and D. J. Mooney, "Alginate: properties and biomedical applications," *Progress in polymer science*, vol. 37, no. 1, p. 106, 2012, ISSN: 00796700. DOI: 10.1016/J.PROGPOLYMSCI.2011.06.003. [Online]. Available: <https://pubmed.ncbi.nlm.nih.gov/pmc/articles/PMC3223967/><https://pubmed.ncbi.nlm.nih.gov/pmc/articles/PMC3223967/?report=abstract><https://www.ncbi.nlm.nih.gov/pmc/articles/PMC3223967/>.

- [47] C. Loebel, S. E. Szczesny, B. D. Cosgrove, M. Alini, M. Zenobi-Wong, R. L. Mauck, and D. Eglin, "Cross-Linking Chemistry of Tyramine-Modified Hyaluronan Hydrogels Alters Mesenchymal Stem Cell Early Attachment and Behavior," *Biomacromolecules*, vol. 18, no. 3, pp. 855–864, Mar. 2017, ISSN: 15264602. DOI: 10.1021/ACS.BIOMAC.6B01740. [Online]. Available: https://www.researchgate.net/publication/313238914_Cross-Linking_Chemistry_of_Tyramine-Modified_Hyaluronan_Hydrogels_Alters_Mesenchymal_Stem_Cell_Early_Attachment_and_Behavior.
- [48] E. Kim, M. H. Kim, J. H. Song, C. Kang, and W. H. Park, "Dual crosslinked alginate hydrogels by riboflavin as photoinitiator," *International Journal of Biological Macromolecules*, vol. 154, pp. 989–998, Jul. 2020, ISSN: 18790003. DOI: 10.1016/J.IJBIOMAC.2020.03.134.
- [49] S. Sakai and K. Kawakami, "Both ionically and enzymatically crosslinkable alginate-tyramine conjugate as materials for cell encapsulation," *Journal of biomedical materials research. Part A*, vol. 85, no. 2, pp. 345–351, May 2008, ISSN: 1552-4965. DOI: 10.1002/JBM.A.31299. [Online]. Available: <https://pubmed.ncbi.nlm.nih.gov/17688281/>.
- [50] P. E. Donnelly, T. Chen, A. Finch, C. Brial, S. A. Maher, and P. A. Torzilli, "Photocrosslinked tyramine-substituted hyaluronate hydrogels with tunable mechanical properties improve immediate tissue-hydrogel interfacial strength in articular cartilage," *Journal of biomaterials science. Polymer edition*, vol. 28, no. 6, pp. 582–600, Apr. 2017, ISSN: 1568-5624. DOI: 10.1080/09205063.2017.1289035. [Online]. Available: <https://pubmed.ncbi.nlm.nih.gov/28134036/>.
- [51] M. Becker, M. Gurian, M. Schot, and J. Leijten, "Aqueous Two-Phase Enabled Low Viscosity 3D (LoV3D) Bioprinting of Living Matter," *Advanced Science*, p. 2204609, 2022, ISSN: 2198-3844. DOI: 10.1002/ADVS.202204609. [Online]. Available: <https://onlinelibrary.wiley.com/doi/full/10.1002/advs.202204609><https://onlinelibrary.wiley.com/doi/abs/10.1002/advs.202204609><https://onlinelibrary.wiley.com/doi/10.1002/advs.202204609>.
- [52] W. Wu, A. Deconinck, and J. A. Lewis, "Omnidirectional printing of 3D microvascular networks," *Advanced Materials*, vol. 23, no. 24, pp. 178–183, 2011, ISSN: 09359648. DOI: 10.1002/adma.201004625.
- [53] G. Štumberger and B. Vihar, "Freeform perfusable microfluidics embedded in hydrogel matrices," *Materials*, vol. 11, no. 12, 2018, ISSN: 19961944. DOI: 10.3390/ma11122529.
- [54] J. Kajtez, M. F. Wessler, M. Birtele, F. R. Khorasgani, D. R. Ottosson, A. Heiskanen, T. Kamperman, J. Leijten, A. Martínez-Serrano, N. B. Larsen, T. E. Angelini, M. Parmar, J. U. Lind, and J. Emnéus, "Embedded 3D printing in self-healing annealable composites for functional patterning of human neural constructs," *bioRxiv*, p. 2021.08.04.455135, 2022. DOI: 10.1101/2021.08.04.455135. [Online]. Available: <https://doi.org/10.1101/2021.08.04.455135><http://biorxiv.org/content/early/2021/08/06/2021.08.04.455135.abstract>.

- [55] W. Cheng, J. Zhang, J. Liu, Z. Yu, and C. Ziyi Yu, "Granular hydrogels for 3D bioprinting applications," *View*, vol. 1, no. 3, p. 20200060, Sep. 2020, ISSN: 2688-268X. DOI: 10.1002/VIW.20200060. [Online]. Available: <https://onlinelibrary.wiley.com/doi/full/10.1002/VIW.20200060> <https://onlinelibrary.wiley.com/doi/abs/10.1002/VIW.20200060> <https://onlinelibrary.wiley.com/doi/10.1002/VIW.20200060>.
- [56] M. E. Prendergast and J. A. Burdick, "Computational Modeling and Experimental Characterization of Extrusion Printing into Suspension Baths," *Advanced Healthcare Materials*, vol. 2101679, pp. 1–14, 2021, ISSN: 21922659. DOI: 10.1002/adhm.202101679.
- [57] K. H. Song, C. B. Highley, A. Rouff, and J. A. Burdick, "Complex 3D-Printed Microchannels within Cell-Degradable Hydrogels," *Advanced Functional Materials*, vol. 28, no. 31, pp. 1–10, 2018, ISSN: 16163028. DOI: 10.1002/adfm.201801331.
- [58] T. Bhattacharjee, S. M. Zehnder, K. G. Rowe, S. Jain, R. M. Nixon, W. G. Sawyer, and T. E. Angelini, "Writing in the granular gel medium," *Science Advances*, vol. 1, no. 8, 2015, ISSN: 23752548. DOI: 10.1126/sciadv.1500655.
- [59] R. Hatti-Kaul, "Aqueous two-phase systems: A general overview," *Applied Biochemistry and Biotechnology - Part B Molecular Biotechnology*, vol. 19, no. 3, pp. 269–277, 2001, ISSN: 10736085. DOI: 10.1385/MB:19:3:269/METRICS. [Online]. Available: <https://link.springer.com/article/10.1385/MB:19:3:269>.
- [60] G.-L. Ying, N. Jiang, S. Maharjan, Y.-X. Yin, R.-R. Chai, X. Cao, J.-Z. Yang, A. K. Miri, S. Hassan, Y. Shrike Zhang, G.-l. Ying, S. Maharjan, Y.-x. Yin, R.-r. Chai, X. Cao, J.-z. Yang, A. K. Miri, S. Hassan, Y. S. Zhang, and B. N. Jiang, "Aqueous Two-Phase Emulsion Bioink-Enabled 3D Bioprinting of Porous Hydrogels," *Advanced Materials*, vol. 30, no. 50, p. 1805460, Dec. 2018, ISSN: 1521-4095. DOI: 10.1002/ADMA.201805460. [Online]. Available: <https://onlinelibrary.wiley.com/doi/full/10.1002/adma.201805460> <https://onlinelibrary.wiley.com/doi/abs/10.1002/adma.201805460> <https://onlinelibrary.wiley.com/doi/10.1002/adma.201805460>.
- [61] Y. Chao and H. C. Shum, "Emerging aqueous two-phase systems: from fundamentals of interfaces to biomedical applications," *Chemical Society Reviews*, vol. 49, no. 1, pp. 114–142, Jan. 2020, ISSN: 1460-4744. DOI: 10.1039/C9CS00466A. [Online]. Available: <https://pubs.rsc.org/en/content/articlehtml/2020/cs/c9cs00466a> <https://pubs.rsc.org/en/content/articlelanding/2020/cs/c9cs00466a>.
- [62] M. Peris, "Sucrose: Properties and Determination," *Encyclopedia of Food and Health*, pp. 205–210, Jan. 2016. DOI: 10.1016/B978-0-12-384947-2.00669-3.
- [63] M. C. Hespanhol, L. H. M. Da Silva, B. M. Fontoura, V. M. De Andrade, A. B. Mageste, and L. R. De Lemos, "Phase Diagrams, Densities, and Refractive Indexes of Aqueous Two-Phase Systems Comprising (F68, L64, or PEO1500) + (Ammonium, Sodium, or Potassium Thiocyanate Salts) + Water: Effect of Cation and Type of Macromolecule," *Journal of Chemical and Engineering Data*, vol. 64, no. 5, pp. 1991–1998, May 2019, ISSN: 15205134. DOI: 10.1021/ACS.JCED.8B01005/ASSET/IMAGES/LARGE/2018-010059{_}0005.JPEG. [Online]. Available: <https://pubs.acs.org/doi/full/10.1021/acs.jced.8b01005>.

- [73] H. J. Butt and M. Kappl, "Normal capillary forces," *Advances in colloid and interface science*, vol. 146, no. 1-2, pp. 48–60, Feb. 2009, ISSN: 1873-3727. DOI: 10.1016/J.CIS.2008.10.002. [Online]. Available: <https://pubmed.ncbi.nlm.nih.gov/19022419/>.
- [74] Y. I. Rabinovich, M. S. Esayanur, and B. M. Moudgil, "Capillary forces between two spheres with a fixed volume liquid bridge: theory and experiment," *Langmuir: the ACS journal of surfaces and colloids*, vol. 21, no. 24, pp. 10992–10997, Nov. 2005, ISSN: 0743-7463. DOI: 10.1021/LA0517639. [Online]. Available: <https://pubmed.ncbi.nlm.nih.gov/16285763/>.
- [75] M. Iqbal, Y. Tao, S. Xie, Y. Zhu, D. Chen, X. Wang, L. Huang, D. Peng, A. Sattar, M. A. B. Shabbir, H. I. Hussain, S. Ahmed, and Z. Yuan, "Aqueous two-phase system (ATPS): an overview and advances in its applications," *Biological Procedures Online*, vol. 18, no. 1, pp. 1–18, Oct. 2016, ISSN: 14809222. DOI: 10.1186/S12575-016-0048-8. [Online]. Available: <https://pubmed.ncbi.nlm.nih.gov/3044470/>.
- [76] M. Mastiani, N. Firoozi, N. Petrozzi, S. Seo, and M. Kim, "Polymer-Salt Aqueous Two-Phase System (ATPS) Micro-Droplets for Cell Encapsulation," *Scientific Reports*, vol. 9, no. 1, Dec. 2019, ISSN: 20452322. DOI: 10.1038/S41598-019-51958-4.
- [77] Y. Jin and H. Yoshino, "A jamming plane of sphere packings," *Proceedings of the National Academy of Sciences of the United States of America*, vol. 118, no. 14, e2021794118, Apr. 2021, ISSN: 10916490. DOI: 10.1073/PNAS.2021794118.SUPPL{1}_FILE/PNAS.2021794118.SAPP.PDF. [Online]. Available: <https://www.pnas.org/doi/abs/10.1073/pnas.2021794118>.
- [78] T. J. Hinton, Q. Jallerat, R. N. Palchesko, J. H. Park, M. S. Grodzicki, H. J. Shue, M. H. Ramadan, A. R. Hudson, and A. W. Feinberg, "Three-dimensional printing of complex biological structures by freeform reversible embedding of suspended hydrogels," *Science Advances*, vol. 1, no. 9, 2015, ISSN: 23752548. DOI: 10.1126/sciadv.1500758.
- [79] D. J. Shiwardski, A. R. Hudson, J. W. Tashman, and A. W. Feinberg, "Emergence of FRESH 3D printing as a platform for advanced tissue biofabrication," *Cite as: APL Bioeng*, vol. 5, p. 10904, 2021. DOI: 10.1063/5.0032777. [Online]. Available: <https://doi.org/10.1063/5.0032777>.
- [80] A. Lee, A. R. Hudson, D. J. Shiwardski, J. W. Tashman, T. J. Hinton, S. Yerneni, J. M. Bliley, P. G. Campbell, and A. W. Feinberg, "3D bioprinting of collagen to rebuild components of the human heart," *Science*, vol. 365, no. 6452, pp. 482–487, 2019, ISSN: 10959203. DOI: 10.1126/science.aav9051.
- [81] Y. Fang, Y. Guo, B. Wu, Z. Liu, M. Ye, Y. Xu, M. Ji, L. Chen, B. Lu, K. Nie, Z. Wang, J. Luo, T. Zhang, W. Sun, and Z. Xiong, "Expanding Embedded 3D Bioprinting Capability for Engineering Complex Organs with Freeform Vascular Networks," *Advanced Materials*, p. 2205082, Feb. 2023, ISSN: 0935-9648. DOI: 10.1002/ADMA.202205082. [Online]. Available: <https://onlinelibrary.wiley.com/doi/10.1002/adma.202205082>.

- [82] Y. Zhang, S. T. Ellison, S. Duraivel, C. D. Morley, C. R. Taylor, and T. E. Angelini, "3D printed collagen structures at low concentrations supported by jammed microgels," *Bioprinting*, vol. 21, Mar. 2021, ISSN: 24058866. DOI: 10.1016/j.bprint.2020.e00121.
- [83] I. Miranda, A. Souza, P. Sousa, J. Ribeiro, E. M. S Castanheira, R. Lima, and G. Minas, "Functional Biomaterials Review Properties and Applications of PDMS for Biomedical Engineering: A Review," 2021. DOI: 10.3390/jfb13010002. [Online]. Available: <https://doi.org/10.3390/jfb13010002>.
- [84] C. Tondera, S. Hauser, A. Krüger-Genge, F. Jung, A. T. Neffe, A. Lendlein, R. Klopffleisch, J. Steinbach, C. Neuber, and J. Pietzsch, "Gelatin-based Hydrogel Degradation and Tissue Interaction in vivo: Insights from Multimodal Preclinical Imaging in Immunocompetent Nude Mice," *Theranostics*, vol. 6, no. 12, p. 2114, 2016, ISSN: 18387640. DOI: 10.7150/THNO.16614. [Online]. Available: [/pmc/articles/PMC5039684/%20/pmc/articles/PMC5039684/?report=abstract%20https://www.ncbi.nlm.nih.gov/pmc/articles/PMC5039684/](https://www.ncbi.nlm.nih.gov/pmc/articles/PMC5039684/).
- [85] G. Yang, Z. Xiao, H. Long, K. Ma, J. Zhang, X. Ren, and J. Zhang, "Assessment of the characteristics and biocompatibility of gelatin sponge scaffolds prepared by various crosslinking methods," *Scientific Reports 2018 8:1*, vol. 8, no. 1, pp. 1–13, Jan. 2018, ISSN: 2045-2322. DOI: 10.1038/s41598-018-20006-y. [Online]. Available: <https://www.nature.com/articles/s41598-018-20006-y>.
- [86] J. Lei, X. Li, S. Wang, L. Yuan, L. Ge, D. Li, and C. Mu, "Facile Fabrication of Biocompatible Gelatin-Based Self-Healing Hydrogels," *ACS Applied Polymer Materials*, vol. 1, no. 6, pp. 1350–1358, Jun. 2019, ISSN: 26376105. DOI: 10.1021/ACSAPM.9B00143/ASSET/IMAGES/LARGE/AP-2019-00143M{_}0008.JPEG. [Online]. Available: <https://pubs.acs.org/doi/full/10.1021/acsapm.9b00143>.
- [87] M. C. Echave, L. S. Burgo, J. L. Pedraz, and G. Orive, "Gelatin as Biomaterial for Tissue Engineering," *Current pharmaceutical design*, vol. 23, no. 24, May 2017, ISSN: 1873-4286. DOI: 10.2174/0929867324666170511123101. [Online]. Available: <https://pubmed.ncbi.nlm.nih.gov/28494717/>.
- [88] A. N. Shvalov, J. T. Soini, A. V. Chernyshev, P. A. Tarasov, E. Soini, and V. P. Maltsev, "Light-scattering properties of individual erythrocytes," *Applied Optics*, vol. 38, no. 1, p. 230, Jan. 1999, ISSN: 0003-6935. DOI: 10.1364/AO.38.000230.
- [89] A. G. Borovoi, "Scattering of Light by a Red Blood Cell," *Journal of Biomedical Optics*, vol. 3, no. 3, p. 364, Jul. 1998, ISSN: 10833668. DOI: 10.1117/1.429883.
- [90] K. P. Ivanov, M. K. Kalinina, and Y. I. Levkovich, "Blood flow velocity in capillaries of brain and muscles and its physiological significance," *Microvascular Research*, vol. 22, no. 2, pp. 143–155, Sep. 1981, ISSN: 0026-2862. DOI: 10.1016/0026-2862(81)90084-4.
- [91] S. Aumann, S. Donner, J. Fischer, and F. Müller, "Optical Coherence Tomography (OCT): Principle and Technical Realization," *High Resolution Imaging in Microscopy and Ophthalmology*, pp. 59–85, 2019. DOI: 10.1007/978-3-030-16638-0{_}3. [Online]. Available: https://link.springer.com/chapter/10.1007/978-3-030-16638-0_3.

- [92] K. Yue, G. Trujillo-de Santiago, M. M. Alvarez, A. Tamayol, N. Annabi, and A. Khademhosseini, "Synthesis, properties, and biomedical applications of gelatin methacryloyl (GelMA) hydrogels," *Biomaterials*, vol. 73, p. 254, Dec. 2015, ISSN: 18785905. DOI: 10.1016/j.biomaterials.2015.08.045. [Online]. Available: /pmc/articles/PMC4610009/%20/pmc/articles/PMC4610009/?report=abstract%20https://www.ncbi.nlm.nih.gov/pmc/articles/PMC4610009/.
- [93] M. Sun, X. Sun, Z. Wang, S. Guo, G. Yu, and H. Yang, "Synthesis and Properties of Gelatin Methacryloyl (GelMA) Hydrogels and Their Recent Applications in Load-Bearing Tissue," *Polymers*, vol. 10, no. 11, 2018, ISSN: 20734360. DOI: 10.3390/POLYM10111290. [Online]. Available: /pmc/articles/PMC6401825/%20/pmc/articles/PMC6401825/?report=abstract%20https://www.ncbi.nlm.nih.gov/pmc/articles/PMC6401825/.
- [94] N. N. Ramrattan, R. G. Heijkants, T. G. Van Tienen, A. J. Schouten, R. P. Veth, and P. Buma, "Assessment of tissue ingrowth rates in polyurethane scaffolds for tissue engineering," *Tissue Engineering*, vol. 11, no. 7-8, pp. 1212–1223, Jul. 2005, ISSN: 10763279. DOI: 10.1089/TEN.2005.11.1212. [Online]. Available: http://hdl.handle.net/2066/47638.
- [95] D. de Jongh, E. K. Massey, A. J. Cronin, M. H. N. Schermer, and E. M. Bunnik, "Early-Phase Clinical Trials of Bio-Artificial Organ Technology: A Systematic Review of Ethical Issues," *Transplant International*, vol. 35, no. October, pp. 1–18, 2022, ISSN: 14322277. DOI: 10.3389/ti.2022.10751.
- [96] J. E. Samorezov, C. M. Morlock, and E. Alsberg, "Dual Ionic and Photo-Crosslinked Alginate Hydrogels for Micropatterned Spatial Control of Material Properties and Cell Behavior," *Bioconjugate chemistry*, vol. 26, no. 7, p. 1339, Jul. 2015, ISSN: 15204812. DOI: 10.1021/ACS.BIOCONJCHEM.5B00117. [Online]. Available: /pmc/articles/PMC6927469/%20/pmc/articles/PMC6927469/?report=abstract%20https://www.ncbi.nlm.nih.gov/pmc/articles/PMC6927469/.
- [97] A. Dodero, L. Pianella, S. Vicini, M. Alloisio, M. Ottonelli, and M. Castellano, "Alginate-based hydrogels prepared via ionic gelation: An experimental design approach to predict the crosslinking degree," *European Polymer Journal*, vol. 118, pp. 586–594, Sep. 2019, ISSN: 0014-3057. DOI: 10.1016/j.eurpolymj.2019.06.028.
- [98] G. Xie, J. Forth, Y. Chai, P. D. Ashby, B. A. Helms, and T. P. Russell, "Compartmentalized, All-Aqueous Flow-Through-Coordinated Reaction Systems," *Chem*, vol. 5, no. 10, pp. 2678–2690, Oct. 2019, ISSN: 2451-9294. DOI: 10.1016/j.chempr.2019.07.016.

A

Schematic overview of experiments needed to build the final construct

Schematic with depicting the workflow regarding experiments and knowledge necessary before building the final construct. The experiments include ATA synthesis, microgel fabrication, MAP formation, emb3D printing for channel fabrication, and pre-saturation studies. Printbath fabrication, ATPS, and perfusion studies are not included (Fig. A.1).

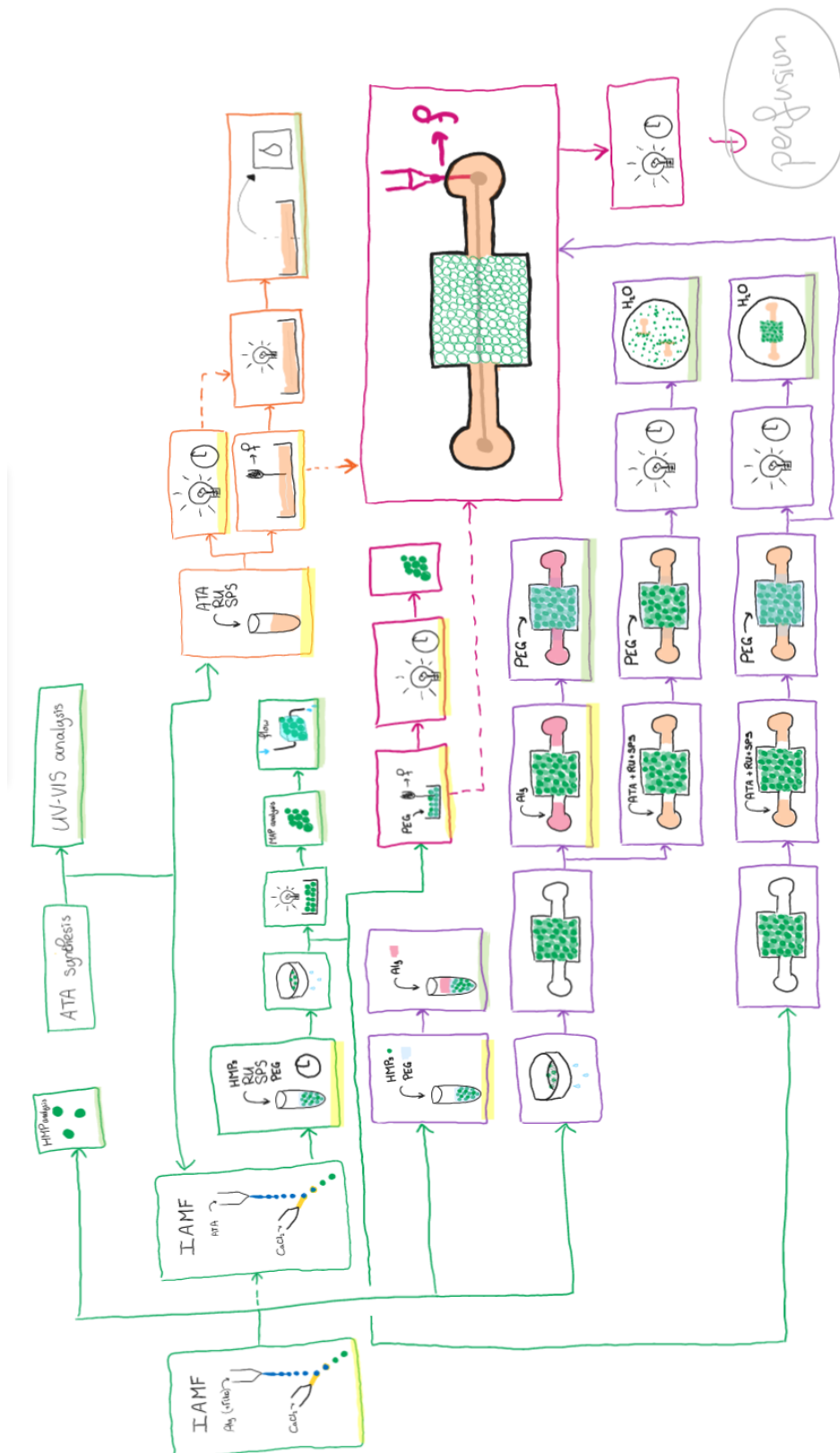


Figure A.1: Green: ATA synthesis, microgel-, and MAP fabrication. Orange: Macroscale channel fabrication through emb3D printing. Pink: Needle movement through microgels. Purple: Pre-saturation studies. Yellow underlined: optimising required.

B

Manual print trials in DexTA

Initially, ATA hydrogel was not suitable candidate for the purpose of macroscale channel fabrication, as the microgels were exposed to an abundance of calcium, which would cause the liquid ATA to crosslink before channel fabrication could take place [46], [96], [97]. Instead, we opted to fabricate channels in dextran-TA (DexTA) [51], [98]. When in later studies it became apparent that the microgels had to be washed and pre-saturated with a polymeric solution, it was decided to abandon DexTA in favour of ATA. This way, the same material is used in the channels and the MAP, and the introduction of additional materials into the structure is avoided.

Nonetheless, manual print trials were conducted by printing through a PDMS bath consisting of three components, where the first and last components are filled with liquid 5% w/v DexTA with 1 unit/mL HRP and the middle component is filled with strained ATA microgels. The sacrificial ink was extruded by a syringe pump (Harvard Apparatus, PHD Ultra, USA) through a 25G needle at a flow rate consisting of 11.23% w/v PEG-35K with 30% H_2O_2 in MQ along with a pipette tip of RhodB granules for visualisation. Due to the presence of HRP and H_2O_2 , the TA functional groups on DexTA crosslink during and after printing, solidifying the DexTA and forming crosslinked ATA microgels.

The presence of a hollow channel was evaluated by taking cross-sectional slices of the printed channel in DexTA with a surgical 22-blade and evaluation under an EVOS microscope. Perfusion through the channel was performed manually by injecting fluorescent particles suspended MQ through a 34G needle. The flow of perfusion particles and further observations were visualised under the EVOS FL microscope.

The results indicated that it was feasible to produce hollow perfusable channels through emb3D printing techniques in liquid DexTA hydrogel. However, during perfusion, it was observed that the hydrogel penetrated the empty space of the MAP due to capillary forces, thus filling up the capillary-like structure. We proposed to resolve this issue by pre-saturating the MAP. As this involves washing the microgels and thus removing excess calcium, it allows us to replace the DexTA with ATA to fabricate the channel through. Following these observations, we had to determine whether it is possible to create hollow perfusable channels with emb3D printing techniques in liquid ATA hydrogel. Also, it is necessary to study the stability of the interface between the MAP and the channel as a time window that allows emb3D printing of a channel through the interface is needed.

C

Additional data from perfusion studies

While it was possible to perfuse the macroscale channel fabricated by emb3D printing, it proved difficult for the perfusion particles to traverse the MAP when it was in a PDMS bath (Fig. C.1A). Instead, it was observed that the perfusion particles preferred to flow on top of the MAP out of the bath, even when a PDMS lid was placed on top of the entire structure (Fig. C.1B).

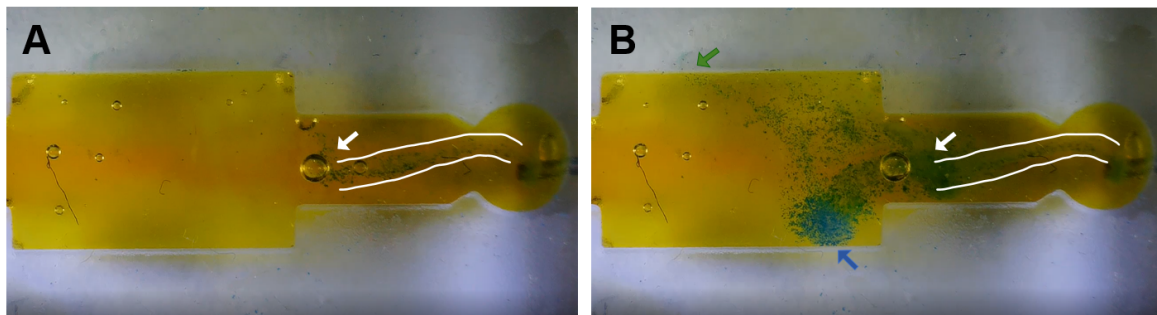


Figure C.1: Perfusion of channel and MAP in PDMS bath with PDMS lid using blue fluorescent particles. White lines around the edges of the channel. White arrows at the bulk-MAP interface **(A)** The perfusion particles have traversed the channel and have reached the beginning of the MAP. **(B)** The perfusion particles have traversed the channel and entered into the MAP-component of the PDMS bath. However, the particles are observed to move alongside the between the MAP and PDMS bath at the blue and white arrows. Also, particles are observed to flow on top of the MAP and go between the PDMS bath and lid.